Experimental Investigation of the Impact Characteristics of Non-Metallic Materials

Final Report

Contract No. NAS8-20346

Control No. DCN1-6-28-0014(1F)

Prepared by: Dr. James L. Hill
Associate Professor of
Engineering Mechanics

and

David W. Cormany
Research Associate

For: University of Alabama
Bureau of Engineering Research
University, Alabama

September 30, 1968

Experimental Investigation of the Impact Characteristics of Non-Metallic Materials

Final Report

Contract No. NAS8-20346

Control No. DCN1-6-28-0014(1F)

Prepared by: Dr. James L. Hill
Associate Professor of
Engineering Mechanics

and

David W. Cormany
Research Associate

For: University of Alabama
Bureau of Engineering Research
University, Alabama

September 30, 1968

This report was prepared by the University of Alabama under Contract No. NAS8-20346 "Experimental Investigations of Impact Characteristics on Non-Metallic Materials," for the George C. Marshall Space Flight Center of the National Aeronautics and Space Administration. The work was administered under technical direction of Research Projects Laboratory, George C. Marshall Space Flight Center, Mr. Stanley A. Fields acting as project manager.

ABSTRACT

Impact tests were performed on solid, vesicular, and granular samples of volcanic pumice and basalt. Characteristic craters were produced for each type of solid sample, and for definite sized ranges of granular material.

The craters in solid basalt are shallow and wide, this due to large spalls being sheared from the craters. The craters in vesicular basalt are produced by direct crushing and by the intense pressure wave generated by impact. These are more conical in profile. The craters in pumice vary greatly with changes in density of the target material. The crater shapes vary from a long, narrow burrow, produced almost entirely by direct crushing action to an impact-shear type crater very similar to these in vesicular basalt with increasing sample density. Empirical quantitative relations were obtained relating certain crater parameters to impact energy and material crushability.

Craters produced at 45 degree angles of incidence are very irregular in plan and very shallow; however, the formation process differs in no substantial degree from that of normal incidence.

In the granular material, three basic shapes of craters were produced. In material less than 125 micron size, the craters are steep-walled with relatively flat floors. These craters have narrow rims and are fairly shallow. In material from 250 to 1,000 microns, distinct double conical craters are produced. In larger sized material, wide, dish-shaped craters are produced. Some quantitative data was obtained for granular impacts. Doubts were raised, however, as to the effects

of the sample containers on the resulting craters in granular material.

Generally, the work performed supports the crater theories of Baldwin and Charters, and extends this theory into a smaller size and energy range than had heretofore been considered.

TABLE OF CONTENTS

INTRODUCTION

There are two basic prevailing theories as to the origin of the majority of the craters covering the lunar surface, those being the speculations of volcanic origin and the proposition of external impacts as the primary cause of such craters. The experiments performed deal with the second of these theories.

Several authorities, among them Baldwin (Ref. 2), Gault (Ref. 4) and Shoemaker (Ref. 8), have sought to establish some means of determination of the origin of craters by classification of a characteristic shape or contour of the crater, and further, to establish mathematical relations allowing some definition of the impacting bodies as functions of varying crater parameters. Shoemaker has also stated that it is possible to distinguish between primary and secondary (those produced by ejecta from a primary crater, the primary crater being produced by a totally alien body) impact craters on the moon's surface by examination of the crater contours.

The experiments performed sought to determine the existance of specific types of craters for impacts in solid and granular volcanic material, the impacts occuring in an evacuated atmosphere, pressure less than 100 microns of mercury, and at velocities approaching lunar escape velocity (i.e. in the range 4,500 to 7,500 fps). In addition, consideration was given to correlating the experimental impacts performed with the theories of Baldwin and Charters (Ref. 3) relating to the ability to define all craters in a given energy range with a single general relation, shifted only by a constant with variation in

the impacted body, and the ability to determine the energy range by examination of certain crater parameters. It was desirous to establish such extension of these theories for smaller laboratory-produced craters, since all other work of this type had been done on much larger craters, either by physical measurement of terrestrial craters centuries after the fact, or from explosively produced craters. In neither case does the process involved duplicate that of the lunar formations, particularly that of secondary lunar crater formation, by reason of both atmospheric presence and energy differences.

Impacts were performed in solid and vesicular basalt, in several types of solid pumice, and in granular samples of pumice and basalt, the granular samples being in concise size ranges from 10 to 4,000 microns. Impacts were also performed at 45 degree angles of incidence in solid samples.

EXPERIMENTAL PROCEDURES

Testing Procedure

The testing apparatus used in the impact testing is shown schematically in Fig. 1. Previous testing (Ref. 1) had shown that there were two main problems associated with the original apparatus, those being the fact that the original projectile accelerator, a .378 Weatherby Magnum action chambered to .30 caliber, could not be dependably loaded to a low enough energy level to avoid shattering the solid samples, and that it produced an unacceptable amount of muzzle blast during each shot.

To alleviate the problem of muzzle blast, a series of experiments was conducted to determine the relative effectiveness of the cryogenic surfaces that were employed to freeze out the products of combustion of the powder. Results of these tests led to discontinuance of use of the LN_2 in the baffle chamber section, retaining only the top and bottom tubes as cryogenic surfaces. This arrangement minimized the muzzle blast effect, but due to the inefficiency of the vertical firing position, a significant amount of solid material, mostly unburned powder grains, was still being fired into the sample along with the projectile, leading to some question as to whether the results produced on the samples were solely due to the projectile. This was particularly noticeable in granular samples. Also, these solid particles, if travelling at a sufficient velocity, could produce unreliable velocity measurements for the projectile, in that they could break the timing wires. There were several cases of this, evidenced by multiple breaks in the timing wires, as opposed to the single, clean break obtained by the projectile alone passing through

the grid. After some experimentation, it was found that by covering the timing boards with two or three thickness of corrugated cardboard, these particles could be prevented from reaching the timing wires. This system proved entirely satisfactory.

Extensive testing was performed with the .30 caliber accelerator in an effort to down-load it to a degree acceptable with respect to shattering of the samples. From these tests, it was deemed impractical, if not impossible to accomplish this. For this reason, a Remington .222 Magnum barrelled action was obtained. This accelerator proved ideal for the desired tests, in that the maximum desired energy ranges could be obtained with near maximum loading of the cartridges, this being the range of maximum efficiency of powder burning. Another advantage of the .222 accelerator lies in the ability to use projectiles of smaller mass (projectiles as light as 6 grains gave excellent consistency) and up-load to fairly high velocities (6,500 to 7,500 fps) while remaining within the desired range of momentum, dictated by the shatter point of the solid basalt samples, about 0.36 lb.-sec. The .222 also produced substantially less muzzle blast than did the .30 caliber, and, with the employment of the procedures outlined above, the problem of muzzle blast was very nearly eliminated.

During the course of the testing, some difficulty was encountered with the velocity timing apparatus, and several instances of very erratic velocity readings were obtained. The source of the problem was traced to the fact that the timing wire grids were grounded to the system itself, and, upon firing the accelerator, the resulting internal vibration of the system was such that it was possible to intermittently break these connections and send spurious signals to the timer, resulting in either erroneous starting or stopping of the counter. Upon installation of an externally

grounded grid system, very consistant and repeatable results were obtained for similar loads and no further problems were encountered with the timing system.

Samples were impacted at incidence angles of 90 degrees and 45 degrees. For the 45 degree shots, only solid samples were used, since artificial packing would have been required to maintain such an angle of repose in the granular samples. The samples impacted at 45 degrees were supported by a system of magnetic blocks and wire loops attached to the base supports. Positioning was critical for the 45 degree shots and it was found to be necessary to bore sight the accelerator on a fixed point marked on the sample before each shot in that configuration.

With the above stated modifications installed in the system, the experimental procedure in making an impact test was as follows:

E1. Place the sample in the impact chamber at 45 or 90 degrees, with appropriate procedural modifications for each configuration.

E2. Load the projectile accelerator.

E3. Evacuate the system to a vacuum of less than 100 microns of mercury (with granular samples, this involves a very slow initial pumpdown and two to four days of pumping time to release and remove trapped air and moisture in the sample).

E4. Fill the shrouds around the upper and lower tubes with liquid nitrogen. This usually causes a pressure drop of 5 to 10 microns, particularly with granular samples.

E5. Institute photographic procedures, if impact photography is to be performed.

E6. Fire the projectile accelerator and impact the target.

E7. Allow the liquid nitrogen to boil away.

E8. Raise the pressure in the system to atmospheric pressure.

E9. Carefully remove the sample from the chamber.

E10. Photograph the sample and note any unusual features concerning either the sample or the ejecta (with granular samples, photographs should be made before removal, as the surfaces are delicate and subject to slumping upon removal).

E11. Perform sample evaluation upon the impacted sample.

Photography

Photography of craters produced was considered an integral part of the testing procedure and was performed immediately subsequent to removal of the sample from the impact chamber for all samples tested. It was also deemed desirable to obtain photographs, both still and motion picture, of the impact process, with specific emphasis to be placed upon establishment of a chronological sequence involved in the impact on various types of samples and identification of, direction of flight, and velocity of individual particles of ejecta if possible. Toward these ends, photographic procedures were established for both still and motion picture photography of the impact process.

Still Photography

Initial efforts at photography of the impact process were with a polaroid-type camera, using an open shutter and providing illumination by means of a single flash from a stroboscope, fired by the breaking of a circuit by the projectile. This sytem failed for a number of reasons, all associated with the camera itself. Among these were inordinately long minimum focal distance of the camera, lack of resolution in the film, no means to produce higher contrast prints with the Polaroid-type film, and a chemical reaction time of the film on the order of milliseconds, while the flash duration is only 3-5 microseconds, resulting in very little being produced on the polaroid film in the way of an image.

The next system used employed a 35 millimeter camera with the same illumination system. This system was operable, but not optimum. The particular camera used had only an f3.5 lens which necessitated using the maximum lens aperture, and obtaining the minimum depth of field. It

also had a rather long minimum focal distance which necessitated some back-off from the desired viewing position and still gave considerable fall-off in sharpness at the edges of the frame.

Finally, a system was established using a Miranda Sensorex 35 mm single lens reflex type camera with a 50 mm f1.9 lens. This system gave excellent results in all respects.

Lighting proved to be a particularly difficult problem. The problem came in the fact that an extremely short duration flash was necessary to "stop" the ejecta, but sufficient illumination had to be present to expose the film and produce relatively high resolution, high contrast photographs. Since the power output of the stroboscope was limited, this ruled out backlighting, or silhouetting of the ejecta particles, since the amount of light penetrating the fine cloud of ejecta was grossly insufficient to expose the film. Sidelighting, at 90 degrees to the view of the camera was attempted, but produced only the outline of the conic cloud being emitted from the sample, not the individual ejecta particles in relief as anticipated; again, this was due to the inability of the limited light source to successfully penetrate the ejecta cloud. The most successful method found within the confines of the impact chamber used was a combination three quarter view, with the strobe light positioned in one angled top port and the camera in the other. This enabled both the camera and light to look "inside" the ejecta cone and view the particles from above as they left the surface of the sample. All of the still shots of the impact process contained herein were obtained in this manner.

The stroboscope was triggered by the projectile breaking a fine wire grid. Initially this grid was suspended above the surface of the sample, but later was attached to the surface of the sample, when photos

taken in the first configuration showed the suspension to be interfering both with the camera view and with the flight of the ejecta particles. The stroboscope itself was equipped with an adjustable internal delay and there was also an external delay unit which allowed variation of the time into impact of the flash from about 100 micro-seconds to more than 1 second in continuous ranges. The delay units were calibrated and it was found that excellent repeatability was obtainable, lending good authority to sequential still photographs of the impact process.

Using the method above, the following procedure was developed for still photography of the impact process:

S1. Prior to placing the sample in the chamber, a fine wire grid was wound on the surface. The ends were soldered to connections leading to the flash unit as the sample was placed in the impact chamber.

S2. Following step E3 of the experimental procedure, the camera was positioned in the viewing port and focused on the sample. A picture of the sample was taken using incandescent lighting in the lighting port.

S3. Following step E4, the desired delay was programmed into the flash unit, the unit was connected to the sample grid, and was positioned in the lighting port.

S4. The camera shutter was opened, step E5 was instituted, firing the flash, and the camera shutter was closed.

S5. An "after" picture was immediately made similar to that of step S2 above.

S6. The film was processed and enlargements were made.

S7. Photographic evaluation was made.

Motion Pictures

Eleven attempts were made to obtain high-speed motion pictures of the impact process. The camera used was a Red Lake Hycam, model K20S4E, 16mm, with a 75mm f2.7 lens. Lighting was provided by two General Electric boron movie lights. After some experimentation, it was found that the optimum lighting conditions were obtained by

letting the camera view the sample in one of the angled top ports with one light in the other angled port and the second in a side port at 90 degrees to the line of sight of the camera. All motion pictures were shot at 5,000 pictures per second. This limitation was imposed by the amount of light possible with the system used. An accurate record of the film frame rate was obtained by using a timing light generator at 1,000 cycles per second. Initially, the camera was positioned at its minimum focal distance from the sample and aligned with the viewing port, a distance of about 3.5 feet. This gave almost no depth of field, and focusing of the lens was extremely critical at this distance; accordingly, on subsequent shots, the camera was positioned on the second level (see Fig. 1) and aligned with the port. Excellent clarity was obtained with this arrangement, although at the expense of some reduction of field of view due to the diameter of the port itself.

Using this method, the following procedure was developed for obtaining high-speed motion pictures of the impact process:

M1. During step E3 above, the camera was positioned and focused, the lights were positioned and tested, and the timing light generator was connected to the camera.

M2. During step E4 above, a light reading was taken, film was loaded into the camera, and the power supply was connected to the camera and timing light generator.

M3. The lights were turned on, the camera started, and step E6 was instituted after run-up of the camera.

M4. The film was removed from the camera and processed.

M5. Photographic evaluation was made, utilizing both frame by frame examination and standard speed projection.

Sample Evaluation

Subsequent to impact, sample evaluation was performed on all samples. In the solid samples, pertinent measurements, such as mean

crater diameters, crater depth, and crater volume were recorded. Any unusual features of the craters were recorded. Apparent density measurements were made for the solid and vesicular basalt samples using a liquid displacement method, and for one type of pumice using the weight of a cut block of regular dimensions.

For the granular samples, contours of the craters were taken, from which profiles of the craters were drawn, allowing determination of rim depth, rim height, wall slopes, crater cross sectional area, and true and apparent (see Ref. 2) crater diameters.

All solid samples were stored; however, as the containers were reused, the granular craters were destroyed.

RESULTS

Impacts were made at normal and 45 degree incidence in solid targets of basalt and pumice. All impacts in granular material were at normal incidence. Results obtained in a quantitative form express crater parameters as functions of projectile energy and material strength. On materials in which insufficient tests were made to draw compelling conclusions of a quantitative nature, the qualitative aspects of the crater formations will be discussed, as will a probable chronological sequence of crater formation for each type of sample impacted. Results are grouped according to sample material.

Solid Basalt-Normal Incidence

Thirteen shots were made on solid basalt samples at normal incidence. The primary feature of the craters in solid basalt samples are the relatively large spalls that are sheared from the craters. The craters themselves are very shallow and wide, having a diameter to depth ratio of 7 to 10. The central regions exhibit evidences of intense shock effects, and in most cases, small shatter cones very similar to those described by Middlehurst and Kuiper (Ref. 5) may be seen in the central region of the craters. In many instances, the spalls may be re-fitted into the craters, and upon such re-fitting, the craters are seen to be roughly polygonal in outline and conical in profile, with an occasional crater being nearly circular. Fig. 7 shows such a crater with some of the spalls having been retained in place by the wire grid attached to the surface to fire the strobe light as described above. This indicates that there is no great amount of force

behind the ejection of these spalls from the craters, a fact further borne out by examination of motion pictures of the impact process. From these, it may be seen that indeed the spalls are the very last major feature formed in the impact process. Chronologically, the impact process is as follows:

1. The projectile strikes the sample. Within 100 micro-seconds, the projectile has started to disintegrate and has crushed the central crater region ahead of itself, generating a very fine cloud of ejecta particles and pieces of the projectile. This cloud departs the surface in a random manner, with seemingly no limiting angle of departure.

2. An intense pressure wave is generated by the impact, and this wave begins to break out small pieces of the sample surrounding the central region. The projectile further disintegrates, and the pieces rebound from the crater.

3. As the pieces of projectile and the small chunks of the target clear the surface, the building shear forces exceed the strength of the material, and the spalls break free and begin to move laterally out of the crater.

4. The intense pressure wave is reflected back through the thickness of the target, throwing the spalls and some very small fragments underlying them upward from the surface of the target. The impact process is now complete. Some material may settle back to the surface of the target following the impact.

An impact photograph is presented in Fig. 6 showing the last stages of 2 above and the beginning of 3. By comparison of Figs. 6 and 7 (the resulting crater from 6), it may be seen that the outlines of the spalls are present at 140 micro-seconds after impact, but the spalls themselves do not appear to have moved. However, many small pieces of the target material and of the projectile may be seen, having already cleared the surface. The remainder of the projectile is still boring into the surface of the target and disintegrating.

Some rather interesting quantitative data for impacts in solid basalt was obtained. This data is presented in Figs. 2 and 3. Fig. 2 is a log-log plot of crater depth as a function of the dimensionless

parameter $\frac{d}{V^{1/3}}$. According to Baldwin (2) and Charters (3) this type of plot gives a measure of the "crushability" or energy absorption capacity of the target material. To the best approximation, this data fits a straight line, and yields the relation:

$$\text{Log}_{10}\, d = 1.57\ \text{Log}\ \left(\frac{d}{V^{1/3}}\right) - 1.140 \qquad (1)$$

Comparison of this relation to a similar one for visicular basalt will be discussed at a leter point.

In Fig. 3 is presented a log-log plot of crater depth vs. projectile momentum. This data fits a straight line to a very close degree, and yields a relation:

$$\text{Log}\ d = 0.51\ \log(mv) - 0.788 \qquad (2)$$

Similar plots for crater volume yield no simple relations as functions of either energy or material strength.

In addition to other testing, one test was performed to determine the size-weight distribution of the ejecta resulting from an impact on solid basalt at normal incidence. A photograph of the sized ejecta is shown in Fig. 38 with total and percentage weight breakdown appearing in Table I. This test revealed that more than 60% of the material removed from the crater area is in the form of particles more than 1,000 micron diameter. Generally, these are the spalled out fragments which produce the characteristic shape of this type crater.

Solid Basalt-45 Degree Incidence

Craters in solid basalt at 45 degree angles of incidence differ considerably in appearance from those at normal incidence, but very

little in process of formation. These craters are very shallow, with depths less than 0.1 inches for the momentum ranges tested. This is due in large part to the fact that the projectile is deflected from the sloping target rather than expending its energy totally in the impact process, as is the case at normal incidence. The resulting craters are very uneven as to profile, and are so shallow as to make judgements as to contour difficult. Most of the spallation occurs in a direction perpendicular to the path of the projectile down the target surface, leaving craters shaped somewhat like the outline of crude "figure eights" oriented at right angles to the projectile flight path. Figs. 8-12 show clearly the formation process for this type of crater. Chronologically, this process duplicates that outlined above for normal incidence. Fig. 8 shows the impact process very nearly completed 1.5 milli-seconds after impact. Note the rather small spalls just leaving the target surface, and that the spalls are among the last of the material to evacuate the crater, the projectile having long since been deflected down the target surface. Figs. 9-11 are prints from one of the high speed motion picture films of the impact process, and in the space of these 24 frames can be followed the entire crater formation, from the impact in the second frame of Fig. 9 to the point at which all material from the crater has cleared the surface in the last few frames of Fig. 11. This film was picked up at a frame rate of approximately 4,000 pps during the final stages of acceleration of the camera. By comparison with the photographs, each of the stages of crater formation outlined above may clearly be seen. Fig. 12 shows the completed crater formed by the impact of Fig. 8. Because of the extreme irregularity of shapes, it was impossible to establish any empirical quantitative relations for the crater formation process similar to those for the normal incidence case.

Vesicular Basalt-Normal Incidence

Nineteen shots were made on vesicular basalt samples at normal incidence. The major characteristic of the crater forming process for these samples was by crushing of the sample by the intense pressure wave propagated through the sample at impact. The craters were characteristically of a crudely polygonal outline and generally were of a fairly uniformly conical profile. The diameter (D) to depth (d) ratio for craters in vesicular basalt was in the range from 2 to 3.75, this figure contrasting to the 7 to 10 range for solid basalt. The inclination might here be to assume that there exists some scale factor relating a $\frac{D}{d}$ range to varying density; however, this does not appear to be so in this case, as the variation in density is not nearly as great as the variation in $\frac{D}{d}$ for the two types. The average density for the solid basalt samples was $2.711 \frac{gm}{cm^3}$ while that for the vesicular samples was $1.8054 \frac{gm}{cm^3}$. Rather, it must be inferred that the variation is a measure of the increased crushability of the vesicular samples. The evidence of this crushability is presented most clearly by the photographic sequence of impacts in vesicular basalt at varying times after impact, shown in Figs. 13-16. Each of these photographs graphically illustrates a distinct phase in the formation of craters of this type. Chronologically, the formation process is as follows:

1. The projectile impacts the target. Almost immediately, a fine cloud of ejecta particles is generated as the projectile crushes the material immediately in its path. The projectile is deformed very little by this initial phase and continues to penetrate the target. This phase is shown in Fig. 13.

2. As the projectile penetrates further into the target, an intense pressure is generated on all sides, crushing the material from

the crater on all sides. The final outline of the crater is now completed as this material is thrown upward from the crater with velocities of the same order of magnitude as that of the projectile. Fig. 14 shows these larger particles leaving the crater area. Note the now completed outline of the crater.

3. The projectile now continues to bore into the central region of the crater, crushing this area out to its final depth; however, it now lacks the energy to disintegrate material in a lateral direction to any significant degree. Hence, the crater narrows to a "point" at the bottom. At this stage, all material classed as ejecta has been thrown from the crater. The remaining material dislodged is compressed into the floor and walls of the crater formed in 2 above. Finally, the remaining body of the projectile rebounds from the crater, and some material ejected from the crater settles back to the target surface. Fig. 15 is a photograph showing the projectile in a clear area boring into the central crater region, all other ejecta having vacated the area around the target.

Fig. 16 shows the resulting crater formed by the impact of Fig. 15. Comparison of Figs. 15 and 16 reveals that no enlargement of the crater was accomplished subsequent to Fig. 15, with the exception of some increase in depth of the crater. Fig. 17 presents a close-up view into a typical crater in vesicular basalt. Note the polygonality of the outer rim, and the discolored, crushed material imbedded in the crater floor. It is interesting to note that, occasionally, a projectile seemed to deviate from its original trajectory after impacting a target, and followed a "path of least resistance," usually breaking into an internal cavity considerably larger than the projectile itself. Such deviations of as large as 30 degrees were observed in at least two instances, and, in both cases, the projectile was lodged in a large internal vesicle of the sample, not having been able to rebound from the crater due to the change in direction resulting in entrapment.

As was the case in the solid basalt, a test was conducted, the primary purpose of which was collection of ejecta for sizing examination. A photograph of the sized ejecta is presented in Fig. 39, with accompanying weight data in Table I. Comparison of the data for solid and

vesicular basalt reveals the more crushable nature of the vesicular material. A considerably smaller proportion of material occurred in the largest ranges for the vesicular basalt, and more material was observed in the intermediate sizes, this material evacuated by the impact pressure blast and crushed somewhat in the process. In the smaller ranges, the differences are primarily due to the lack of solid resistance to the projectile providing an impediment strong enough for pulverization of material on the part of the vesicular material.

Similar relations as those of Eqs. (1) and (2) for solid basalt have been obtained for vesicular basalt impacts. These are presented in Figs. 2 and 3. In this case, the corresponding equation to (1) is:

$$\text{Log } d = 1.57 \text{ Log } \left(\frac{d}{V^{1/3}}\right) - 1.033 \qquad (3)$$

and the corresponding equation to (2) is:

$$\text{Log } d = 0.51 \text{ Log}(mv) - 0.310 \qquad (4)$$

It should be noted that the slopes for corresponding relations are indentical, implying that there exists some general form of relation for depth of craters as functions of momentum and target strength which is a characteristic only of the energy level of impact, with material changes only tending to shift the curve. This same type of argument is propounded rather extensively by Baldwin, and, to a lesser degree by Charters, although all other work is done in a much larger size and energy range. All evidence here presented would tend to support these theories. As was the case with the solid basalt, investigation of relationships involving volume and diameter produced no such simple relations as functions of momentum and/or target strength.

Vesicular Basalt-45 Degree Incidence

There exists very little difference in the craters formed at a 45 degree incidence in vesicular basalt and those formed at normal incidence with respect to method of formation. In physical appearance, the only differences appear to be in the slopes of the crater walls, and, to some degree, the crater outline. The "downhill" walls are very steep, at times approaching perpendicularity to the target surface, while the "uphill" walls are of a fairly shallow slope, on the order of 20 to 30 degrees relative to the surface. The craters are somewhat elliptical in plan, due to the incidence angle, but remain basically conical in profile. This, again, is indicative of the increased crushability of the vesicular samples, in that the projectile is retained to a much greater degree rather than being deflected from the target surface. An insufficient number of impacts was performed to obtain quantitative relations for these impacts.

Pumice

Five types of solid pumice samples were impacted, these types ranging in density from approximately 0.35 gm/cc to 1.8 gm/cc, this upper limit approaching the density of vesicular basalt. Each type yielded a very distinct crater shape and, when considered as a sequence, a pattern of crater shapes emerges. The least dense of these samples totally failed to impede the progress of the projectile, which completely penetrated the samples (samples were 4 inches in thickness) with very little deformation, leaving a burrow very close to projectile diameter through the sample. The shape of the other four types are shown as a photographic sequence in Figs. 18-21.

Fig. 18 shows the crater produced in rather coarse grained pumice of density 0.65 gm/cc. The crater consists of a deep, narrow burrow

approximately twice the diameter of the projectile and two inches deep. The projectile may be seen resting at the bottom of the burrow. This crater is produced entirely by crushing action of the projectile. Samples of sufficient porosity, such as this, allow escape of the pressure wave normally generated by impact; this accounts for the narrow nature of the crater. Extremely little material is thrown out of a crater of this type, but is rather compressed into the sides and bottom of the crater preceding the projectile.

In pumice having a density of approximately 1 gm/cc, the crater shown in Fig. 19 is of a markedly different shape. This crater, while still fairly deep, is elliptic in nature, indicating a decrease in porosity causing retention of the pressure blast within the crater, this in turn producing the ellipticity of the crater and ejecting a significant amount of material from the crater. The projectile may be seen in the crater, but it is not resting on the bottom of the crater. Rather, the projectile appears to have rebounded to some degree, and then fallen back to its final position. The amount of material retained in the crater is not substantially different from that remaining in the crater of Fig. 18, being 36 grains in weight and 30 grains, respectively.

The third type of crater, and possibly the most familiar type of crater to be found in crushable material, is shown in Fig. 20. This crater has a small entry hole of about two projectile diameters opening into an almost perfect elliptical interior. The crater is much more shallow, only 1.2 inches deep. The sample density is 1.37 gm/cc. This crater is produced mainly by the impact pressure blast. This blast is shown most graphically in Fig. 23, an impact photograph of the crater of Fig. 20, taken 880 micro-seconds after impact. Note that the intense pressure has opened small jets at points several projectile diameters

from the entry hole, with material being vented from all of them, as well as from the entry hole itself. These small jets are very characteristic of material of this type, appearing in all of the samples impacted. Nonetheless, substantial amounts of material remain in the crater, being extremely compacted and adhered to the entire internal surface of the crater. Twenty one grains of such compacted material were removed prior to making the photograph of Fig. 20.

The final type of pumice crater is shown in Fig. 21. This crater is more like that produced in vesicular basalt than like the pumice formations of the preceding cases. It is produced by a combination of impact pressure and shear forces, producing some spallation. Again, however, substantial amounts of compacted material remain adhered to the crater walls. There is one feature peculiar to this type of pumice crater which was produced in no other samples tested. This is the appearance of a central crater elevation. This elevation, visible in Fig. 21 and shown in close-up view in Fig. 22, was produced in each of four samples of this type impacted, all such elevations being very similar in appearance. The elevation is round, has a height of approximately 0.125 inches above the crater floor, and is flat topped. It does not consist of compacted material compressed into the crater floor, but is firmly attached, indigenous crater material.

Thus the pattern emerges; from deep narrow burrow, to elliptical burrow, to shallow ellipse, to the impact-shear crater with increasing sample density, the crater shape is governed by the ability or the target to retain the pressure blast following impact as well as the degree of crushability of the target.

Granular Basalt

It is in the area of impacts in granular samples that some correlation of photographic evidence with lunar craters may be made. Examination of the resulting craters in granular material shows several trends.

In the basaltic material of less than 125 micron size, the craters are shallow, steep-walled, and exhibit rather flat floors. The crater rims are only slightly raised, and this raised effect is of a very narrow nature, being more like a precipitous band surrounding the crater, dropping steeply and sharply to the crater floor. Figs. 24-26 show three views of such craters. Note in Fig. 25 the sharp rise and drop of the rim. Another interesting feature of craters in this type material is the considerable amount of agglomeration of material on the surface. These agglomerated "lumps" are uniformly distributed over the surface, both within the crater and in the area surrounding the ramparts. There is no evidence of fold or flow lines indicative of post formation slumping in these craters, but from general appearances, specifically the texture and color of the floor material at the outside of the crater as opposed to that at the center, there exists at least a very good possibility that the formative process involved simultaneous collapse of overhanging rims during the impact process, the original shape being more on the order of the crater in solid pumice shown in Fig. 20 and the material lacking the cohesiveness to sustain such a shape. The resulting collapse, dumping material into the crater, would tend to account both for the flat floors and the steep walls. This inner ring of material is clearly visible in the photographs.

A high speed motion picture was made of the impact process in the crater of Fig. 26, and, though the field of view was too small to verify the hypothesis above, the film did show several very interesting features

of the impact process for such materials. The most unusual feature of the impact is that it does not appear to be a smoothly continuous process, but is rather of an impulsive nature, with three or four distinct phases. These are:

1. As the projectile strikes, a dish-shaped crater is immediately formed. This crater begins to expand uniformly, and large amounts of material are blown out in a conic pattern, the angle of the cone relative to the target surface being 40-60 degrees. This initial crater very soon (20 milli-seconds) reaches a limiting size, however, and for a time, very little motion is observed on the target surface, and almost no material is ejected from the crater.

2. This initial crater begins to decay, as though a force were being exerted on it from within the sample tending to "turn it inside-out." Within this phase, there are several separate, impulsive discharges of material from the crater, in random directions. The impact process has, at this point, been in progress about 100 to 125 milli-seconds.

3. Following the second phase, there occurs a rather unusual looking phase, about which there is some doubt as to cause. The central impact region begins a sudden and very rapid (approaching the impact velocity of the projectile) displacement of material in a lateral direction, with tightly spaced concentric ripples surrounding the impact point expanding very rapidly away from the impact point. Immediately, the base of the projectile is made visible by the evacuation of material surrounding it, but the projectile is not continuing into the target; rather, it is either being thrown from, or, is rebounding from the crater. As the lateral displacement of material continues, there is very little evidence of material being actually ejected from the target surface. The projectile clears the target surface.

4. The projectile is now tumbling immediately above the impact point. the impact process is approximately 250 to 300 milli-seconds after impact. Very suddenly, the target surface, until now appearing to be more fluid than solid, solidifies, seeming to "freeze" in position. The agglomeration of material is simultaneous with this phase. The projectile settles back to the crater floor, being more than half buried by its own momentum. A small amount of material remaining above the crater falls back to the surface, and the impact process is completed. From impact to completion, almost one half second has elapsed.

There are two possibilities as to the cause for the events described in steps three and four: Either it is a natural phenomenon peculiar to impact craters in this type of material, or it is an artificially induced effect due to the apparatus used. These possibilities will be more fully

discussed at a later point.

Another occurrence peculiar to this type material was the formation of a hard, compacted cone of material on the impacting face of the projectile. This formation occurred on all shots made in granular basalt less than 125 micron size and in no other instances. This type formation is shown in the inset to Fig. 26.

The second type of crater produced in granular basalt, occurring in material from 125 to 500 micron size, is the double conical shape, shown in Figs. 27 and 28. These craters are characterized by a definite central conic crater, surrounded by a large, dish-shaped crater. Both craters have smooth contours and marked raised rims. In contrast to the smaller particle size, there is almost no agglomeration of material for this type. The dominant characteristics of these craters are the smooth continuity of all features. There are no sharp breaks or steep slopes, only gently rounded raised rims sloping smoothly to the crater floors.

In material larger than 500 microns, the inner crater disappears, leaving a large dish-shaped crater having smooth contours and a very circular plan. Such a crater is shown in Fig. 29. These craters are fairly deep and possess low, wide rims, unlike the previous cases in which the rims were higher relative to the crater depth and considerably more narrow relative to the crater diameter.

Examination of Ref. 1 reveals quite a different type of crater formation in similar material with a different type of projectile, but within the same momentum range. Possible causes for this will be discussed later.

Granular Pumice

Of the fourteen tests conducted in granular material, six were in granular pumice. One shot each was fired in 10-37 and 37-63 micron size

ranges and the remaining four were in 62-125 micron size, varying projectile momentum to ascertain the changes in crater parameters. As was the case in the granular basalt tests, craters were typed in size ranges. However, the corresponding crater shapes in the pumice samples were not of corresponding ranges, but were of smaller sized material.

In the 10 to 37 micron sample, a stable crater was formed of the type hypothesized for the finely ground basalt. The crater had a circular entry hole approximately two inches in diameter opening into a larger internal cavity. The crater was stable in this configuration, but was very delicate. In attempting to remove the sample from the chamber, the crater overhangs collapsed into the crater, yielding the resulting formation shown in Fig. 30. This crater resembles very much those in the 37-125 micron range in the basaltic material, in that it has a relatively flat floor, very steep walls, and slightly raised rims terminating sharply in the drop to the crater floor. This supports to a considerable degree the hypothesized simultaneous collapse of overhangs in the previous case. There are, though, considerable differences between the craters in the two different types of material. The pumice crater possesses a very distinct and well formed ray system. This system is very evident in Fig. 30. The pumice crater is also much deeper than those found in either of the basaltic ranges, being nearly three inches deep, as opposed to the average of about 1.75 inches for the basalt. Fig. 31 shows a close-up view of the rim of the crater. In this photograph can be seen the beginning of the ray system, and, of particular note, the steepness of the walls and the compacted fractures, rather than slumping, which produced the collapse of material into the crater. It may be seen that the material which did collapse into the

crater is highly agglomerated, seeming to consist of individual lumps or clods, rather than as a mass.

A motion picture was made of this impact, and it shows much of the same type of formation as that in the previously detailed basalt case. The formation of the crater in this case is also impulsive in nature, with at least three separate discharges of material from the crater interspersed with periods of either relative inactivity or lateral movement of the target surface. However, the projectile did not rebound from the crater in this case, and the lateral movement of material was neither as rapid nor as significant, mass-wise, as that in the basaltic case. The camera view of this impact was somewhat hindered by the increased amounts of material ejected from the crater in the initial phases of formation blocking out the light sources, and, hence, not as detailed an account of the crater formation can be presented.

The crater produced in the 37-63 micron size is very similar to both the collapsed 10-37 micron pumice crater and to those in the finely ground basalt. The surface contour is smoother than in the previous pumice crater, with the material around the outside walls forming a small hump, as though a bisected torus were resting in the crater. This crater, however, did not have the appearance of a double cone, as the central region was very nearly of the same depth as the floor immediately at the base of the walls.

The craters produced in the 62-125 micron pumice should be considered as a group, with emphasis placed on changes in the crater characteristics as a result of changing momentum. All of the craters in this material are distinctly double conical, and all are within 1% of the same rim diameter. Figs. 32-37 demonstrate the physical variation of the crater shapes with increasing energy. The most significant of these are:

1. Decreasing contour smoothness with increasing momentum. In the low energy impact (Figs. 32 and 33), the contours of the crater are all smoothly curved. The raised rim bordering the inner crater rises smoothly from the large crater floor and the slope into the inner crater is very continuous. Note also the smooth, very distinct ray pattern evident around the inner cone, but that the rays are absent from the ramparts of the large crater. There is some evidence of agglomeration of material, with most of the agglomerated lumps occurring on the upper slopes of the larger crater.

2. Decreasing diameter and increasing depth of the inner crater. In comparing Figs. 32, 34, and 35, it is easily seen that the diameters of the inner cones are decreasing considerably, but still are remaining basically circular. The depths of these inner craters are .75 inches, .85 inches, and .95 inches respectively.

3. The appearance of a "hardened" surface with increased momentum. The craters of Figs. 34-37, in a higher energy range, have a surface which has formed a "crust" over it. This state is responsible for the very sharp breaks into the inner craters of these samples, as shown in Figs. 36 and 37. Fig. 37 actually shows a slight overhang into the central crater for the highest energy shot of this group.

4. Shifting of position of agglomerated material. The small lumps appearing in the higher energy shots are closer to the inner crater rims than were those of the lower energy case. The probable explanation of this comes from consideration of the variation of contour of the inner craters. The inner crater of the lowest energy shot is more of a hemispheric nature, while the other two are nearly conical. If these compacted masses of material were produced by compression ahead of the projectile, as is reasonable to assume, then the smaller slope of the inner crater in the lower energy shot would allow a lower trajectory, giving more distance, than would the steeper-walled craters following, if the material was ejected from the floor of the inner cone.

5. The appearance of post-formation slumping in the higher energy shots. The evidence of this type of action is very clearly shown in the photographs. The fold or flow lines are very evident in the central craters for both of the higher energy shots, but none are present in the low energy case. This would indicate that in the higher energy shots, very steep walled inner craters are formed. These craters have slopes greater than the angle of repose even of the compacted material in which they are formed. Therefore, as the impact process is being completed, and the pressure wave subsides, or possibly as a rarefaction wave is reflected back through the material, these slopes collapse and flow into their maximum angle of repose, producing the crater shapes seen in the photographs.

In addition to these physical changes, some quantitative data was assembled for these craters. Figure 4 gives the variation of volume of

the craters in 62-125 micron granular pumice as a function of projectile momentum. In Figure 5 is presented a relation which lends increased authority to the fluid-type impact described above. Figure 5 is a log-log plot of crater depth versus momentum for the 62-125 micron pumice samples and for the basaltic samples of a size range greater than 1,000 microns. Comparison of this curve (noting that in a linear scale, the curve would be even more pronounced) to the results given by Charters (Ref. 3) indicates that these impacts are taking place in the transitional range of fluidic impacts, between the case of simple impact force produced craters, and the hypervelocity range, in which the projectile vaporizes and the resulting crater is comparable to an explosively formed crater.

DISCUSSION OF RESULTS

Several points of interests, as well as possible evidences of deviation from expected and/or usual behavior were observed during the course of the investigation. While it would not be correct to attempt to expand limited deviations of a single or, at most, two or three occurrences, to a generalized statement, these deviations do merit mention and some discussion. Also, there were some cases in which two possible alternatives exist as to a cause-effect relationship for a repeated occurrence, and it was impossible to determine the true cause. These cases, too, merit discussion. It is this type occurrence which will be here presented.

Solid Samples

Actually, there were two types of vesicular basalt made available for testing; but, since the second, denser, type was made available at a time when the programmed sequence of impacts in vesicular basalt had been completed, only one shot was made in this type. It did, however, show up an interesting possibility, one which was further supported by two tests made in pumice samples. The results of this test would indicate that as the relative volume of the vesicles decreased, a continuous shift in crater formation would take place from the crush-produced conic form typical of vesicular basalt to the impact-shear type of the solid basalt. This implies, at least, that there exists a limiting point, which should be definable, at which spallation would occur with further decreasing vesicular volume. Such definition would allow classification

of densities by examination of the type craters produced, given some knowledge of the impacting body. Conversely, given a knowledge of the density ranges of a material, examination of the crater type would provide some indication as to the energy of the impacting body, and coupled with the relations given above in Eqs. (2) and (4) could give a rather good definition of such a body.

This same type of reasoning is also true for the pumice material, and indeed, in the pumice tests, this limit was passed and spallation-dominated craters were produced.

There was evidence that in the pumice samples, the projectile trajectory relative to the grain direction of the target influenced the crater shapes to a significant degree. The supporting evidence for this comes from the two shots fired into solid pumice samples at a 45 degree angle of incidence. In both cases spallation was produced. While it would be expected that this would be the case with one of the samples, of the densest type, it was not expected in the second case. This sample was of the type shown in Fig. 19. The main body of the crater was still of the same nature, but the entry hole had been greatly enlarged by the shearing out of spalls, which, when refitted into the crater, gave an almost identical crater to that of Fig. 19. Since only two tests of this type were performed, it was not considered conclusive to a degree to merit formal presentation, but there is the implication, at least, of marked crater changes in crushable materials with changes in orientation of grain lines relative to the impact trajectory.

Granular Samples

As data reduction proceeded for evaluation of the craters produced in granular material, it became evident that there existed a reasonable doubt as to the validity of any generalized conclusions expandable to

conditions other than those under which the specific impact was conducted for crater formations in granular material. These doubts are prompted by several occurrences and/or "coincidences," these same coincidences appearing to show up also in work of the same type performed by Gault, et. al. (Ref. 4).

First among these occurrences is the remarkable recurrence of craters having almost exactly the same rim diameter, while the impacting projectile momentum varied as much as 50%. This recurring diameter situation was evident for each material in which more than one impact was conducted, and in groups of similar materials as well. In examining the work of Gault (Ref. 4), it is notable that from all appearances, that in similar materials, he, too, produced craters very nearly the same diameters, even while varying the angle of incidence of the impacts.

The second item is that of the double conical crater. In a survey of published literature dealing with impact studies, in no case was there found a mention of a consistently produced crater bearing even a familiar resemblance to the repeated double conics described above. There were cases of central burrows in solid targets, but in all cases of granular targets, laboratory produced craters were more or less of the shape of those of Fig. 29.

The third item is the impulsive nature of the crater formation and the observed lateral displacement of material and subsequent rebound of the projectile evidenced in the high speed motion pictures of several of the granular samples.

The obvious connection relating all of these features, a question which has not been answered, is this: In the formation of all laboratory produced craters, to what extent does the confinement of the target material in a limited container influence the resulting crater?

There are only two possible explanations for each of these occurrences. Either they are a natural phenomenon, in which case all such craters should obey the same laws and restrictions, or they are an artificially produced feature, generated by the testing apparatus. It would seem doubtful that true double conical craters would be consistently produced in one case and not in another, were only natural phenomenon acting in such production. Rather, it might be suggested that the influencing factor involved is the depth of the material being impacted. The craters produced by Gault bear much resemblance to the larger craters described above, but the sample depths were considerably less. The obvious question then is as to whether the increased depth is the responsible factor for the double conical shape. This is a question which should be answered.

Regarding the question of similar diameters, it is almost compelling to acknowledge the effects of the containers on the craters. In no case did the rim slope of a crater return to the horizontal within the confines of the container. From his photographs, the same is true of the work of Gault. Another question is posed as to the effect of an immovable, energy reflecting barrier imposed within the sphere of influence of the impacting projectile.

This same effect, that of energy reflection, offers the best explanation of the impulsive formation of the granular craters, and offers visual evidence that there is some container effect. The continuous reflection of pressure waves from the floor and walls of the surrounding container would very well explain both the impulsive nature and concentric motion of material evidenced in the formation of the granular craters. A third question arises as to the process of crater formation in the absence of such restrictions.

These questions cannot easily be answered, but without answers, there

is at least a reasonable doubt as to the validity of expansion of laboratory produced impact data to a general case.

There is one further occurrence which merits discussion. In previous work, using a larger caliber projectile (Ref. 1), several craters were produced in granular basalt of a size range similar to those of Figs. 24 to 26. The resulting craters bore very little resemblance to the ones described above, but were deep, hemispherical pits, with very little evidence of raised rims. The momentum ranges for the two impacts were very nearly the same. This raises the possibility of a size effect relating the size of the impacting projectile to the mean grain size of the impacted material. The hemispherical craters were reproducible with the larger caliber accelerator, as were the flat-floored craters with the smaller caliber in the same energy range. Determination of such a size effect would allow increased definition of an impacting body producing a measurable crater in a known material.

CONCLUSIONS

From the experiments performed, it may be concluded that there are definite types of craters associated with specific materials subjected to impacts in a given energy range. The data gathered supports the theory of Baldwin and Charters that there exists a general relation for all craters produced in solid materials which is a function only of the impacting energy, and that difference in materials tends only to shift the reference origin for the relation.

It was found that in granular samples, such types also existed, and some quantitative data further supported the fluid impact theory of Charters. However, it is deemed necessary to acknowledge that there is some influence in the formation of the granular craters due to the confinement of the samples within containers.

Generally, the experiments performed may be considered an extension of the general crater theory into a much smaller scale impact range than had heretofore been considered, such theory being upheld for the craters produced and the energy ranges considered.

REFERENCES

1. Hill, J. L. "Experimental Investigation of the Impact Characteristics of Non-Metallic Materials," Annual Report No. 1, NAS8-20346, University of Alabama, 1967.

2. Baldwin, R. B. The Measure of the Moon. University of Chicago Press, 1963.

3. Charters, A. C. "High Speed Impact." Scientific American, Vol. 203, p. 128, 1960.

4. Gault, Donald E., Quaide, William L., and Oberbeck, Verne R. "Interpreting Ranger Photographs from Impact Cratering Studies." From proceedings of the 1965 IAU-NASA Symposium on the Nature of the Lunar Surface. Baltimore, The Johns-Hopkins Press, 1965.

5. Middlehurst, Barbara M., and Kuiper, Gerald P., ed. The Solar System. Vol. IV. Chicago University Press, 1963.

6. Kopal, Z. An Introduction to the Study of the Moon. New York, Gordon & Breach, 1966.

7. Salisbury, J. W. & Glasser, D. E., ed. The Lunar Surface Layer. New York, Academic Press, 1964.

8. Shoemaker, E. M. "Interpretation of the Small Craters of the Moon's Surface Revealed by Ranger VII." Proceedings of International Astronomical Union. Hamburg, Germany, 1964.

APPENDIX A

TABLE I

Reference to Figs. 38 and 39

	Solid Basalt	Vesicular Basalt
Total ejecta weight	110.4 gr.	98.8 gr.
Less than 44 micron	3.2 gr.	00.8 gr.
44-63 micron	2.8 gr.	4.4 gr.
63-125 micron	7.1 gr.	5.1 gr.
125-250 micron	8.0 gr.	7.4 gr.
250-500 micron	11.4 gr.	13.8 gr.
500-1,000 micron	14.65 gr.	15.7 gr.
Greater than 1,000 micron	64.25 gr.	51.6 gr.
Percentage Weight		
Less than 44 micron	2.89	0.80
44-63 micron	2.53	4.45
63-125 micron	6.43	5.16
125-250 micron	7.24	7.48
250-500 micron	10.32	13.96
500-1,000 micron	13.26	15.89
Greater than 1,000 micron	64.25	51.6

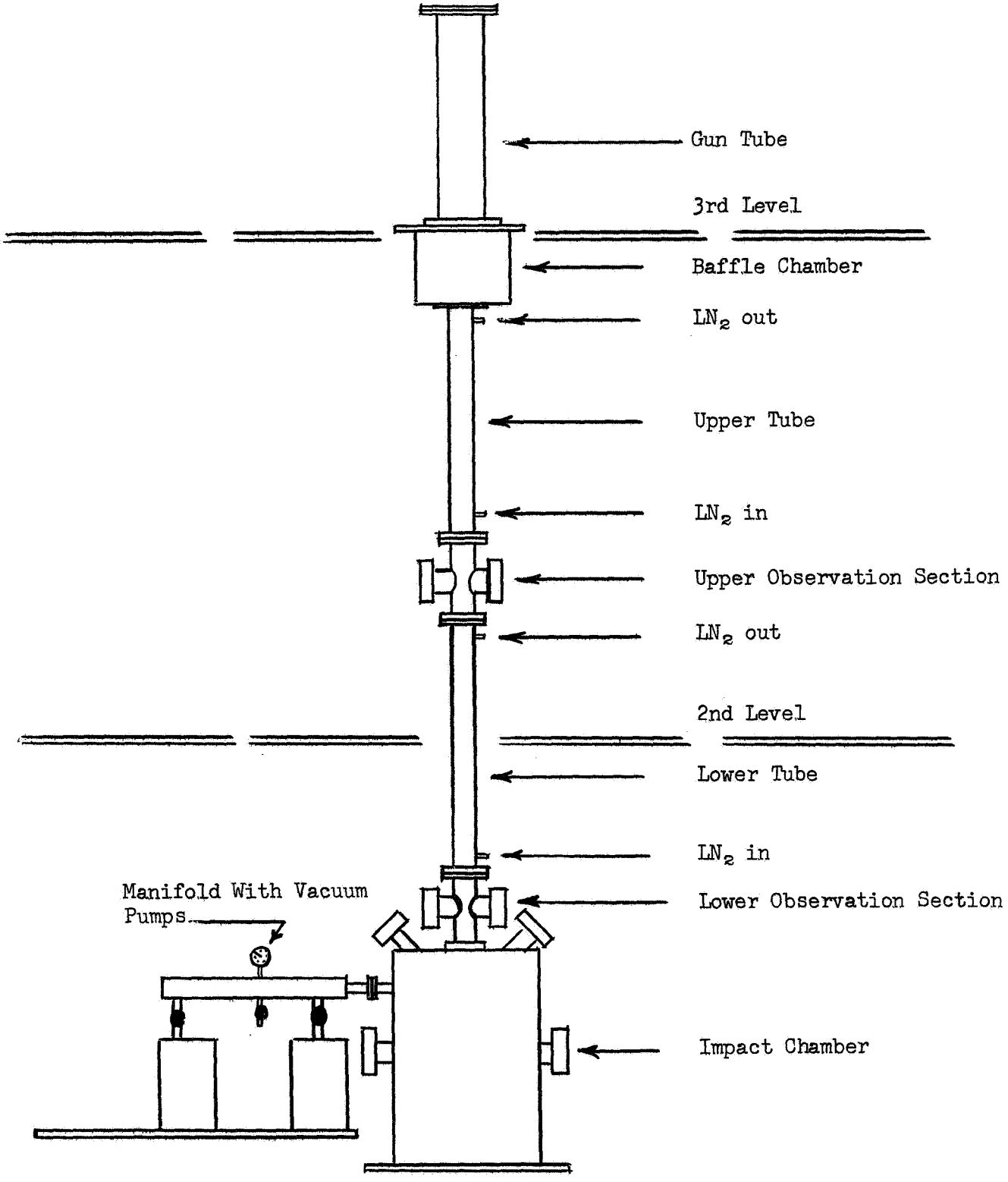

Sketch of Impact Chamber System

Fig. 1

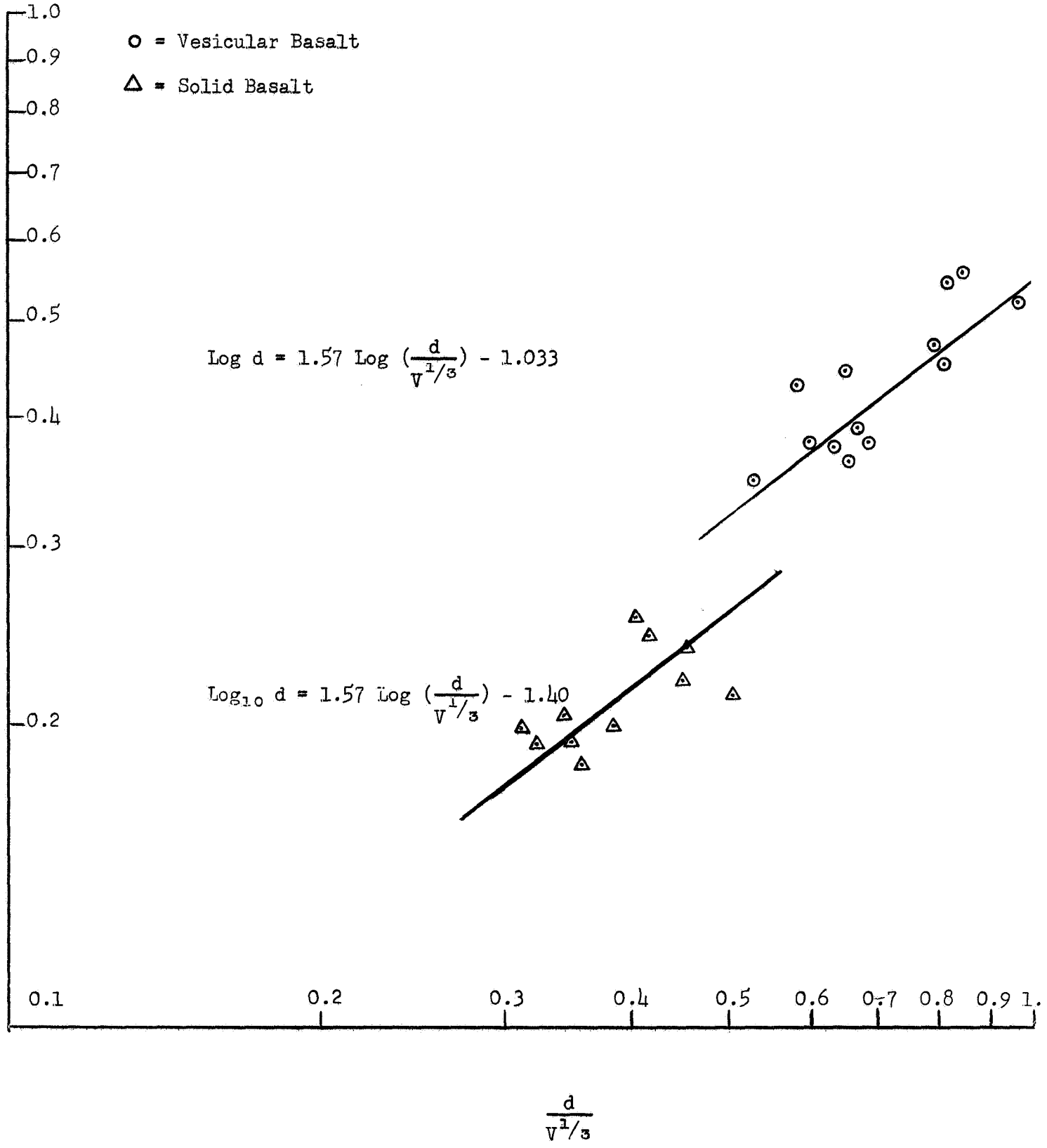
1.0
0.9
0.8
0.7
0.6
0.5
0.4
0.3
0.2
○ = Vesicular Basalt
△ = Solid Basalt
Log d = 1.57 Log (d / V^1/3) - 1.033
Log10 d = 1.57 Log (d / V^1/3) - 1.40
0.1
0.2
0.3
0.4
0.5
0.6
0.7
0.8
0.9
1.
d / V^1/3

Fig. 2

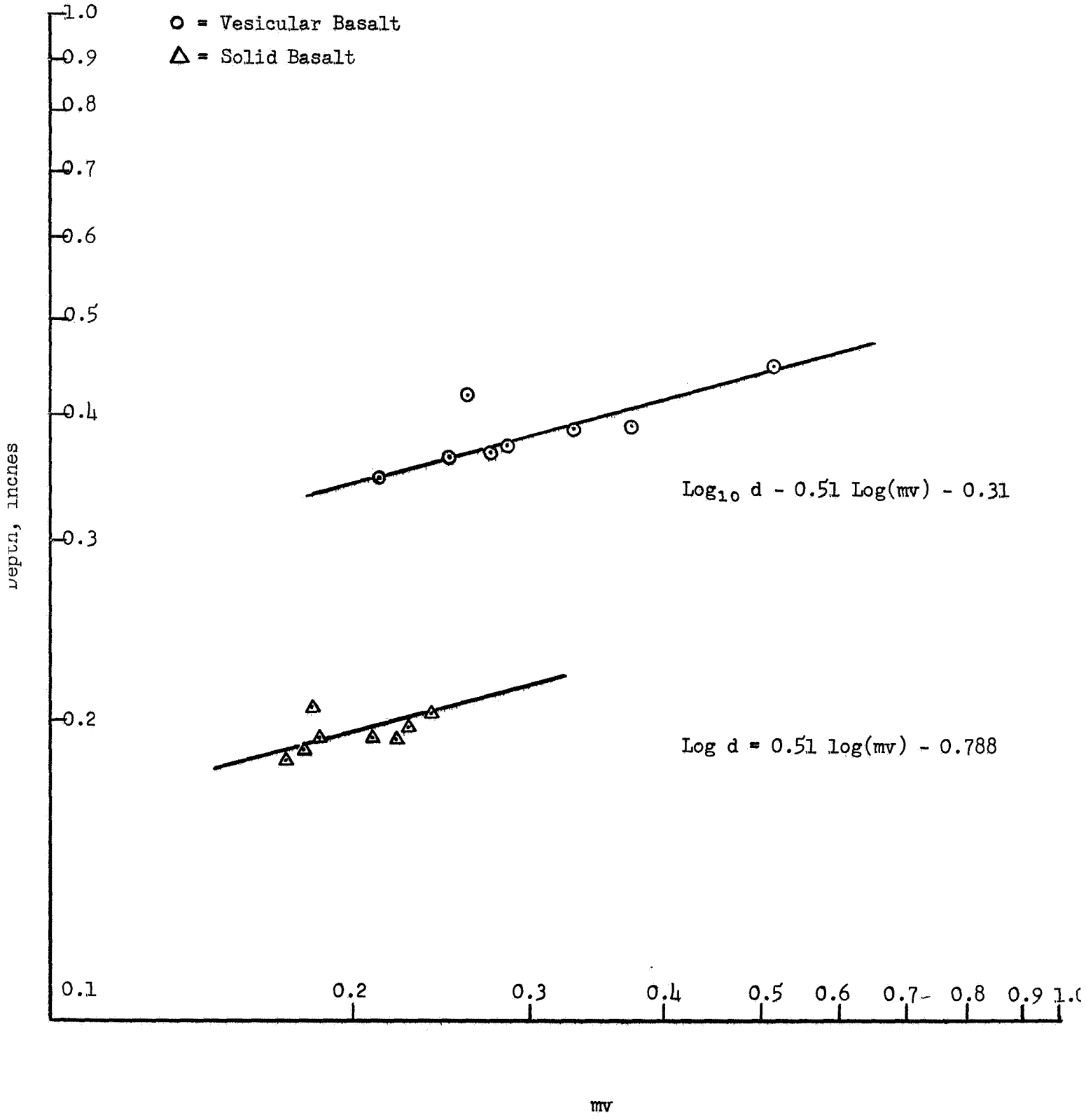
O = Vesicular Basalt
Δ = Solid Basalt
Log10 d - 0.51 Log(mv) - 0.31
Log d = 0.51 log(mv) - 0.788
Depth, inches
mv
1.0
0.9
0.8
0.7
0.6
0.5
0.4
0.3
0.2
0.1
0.2
0.3
0.4
0.5
0.6
0.7
0.8
0.9

Fig. 3

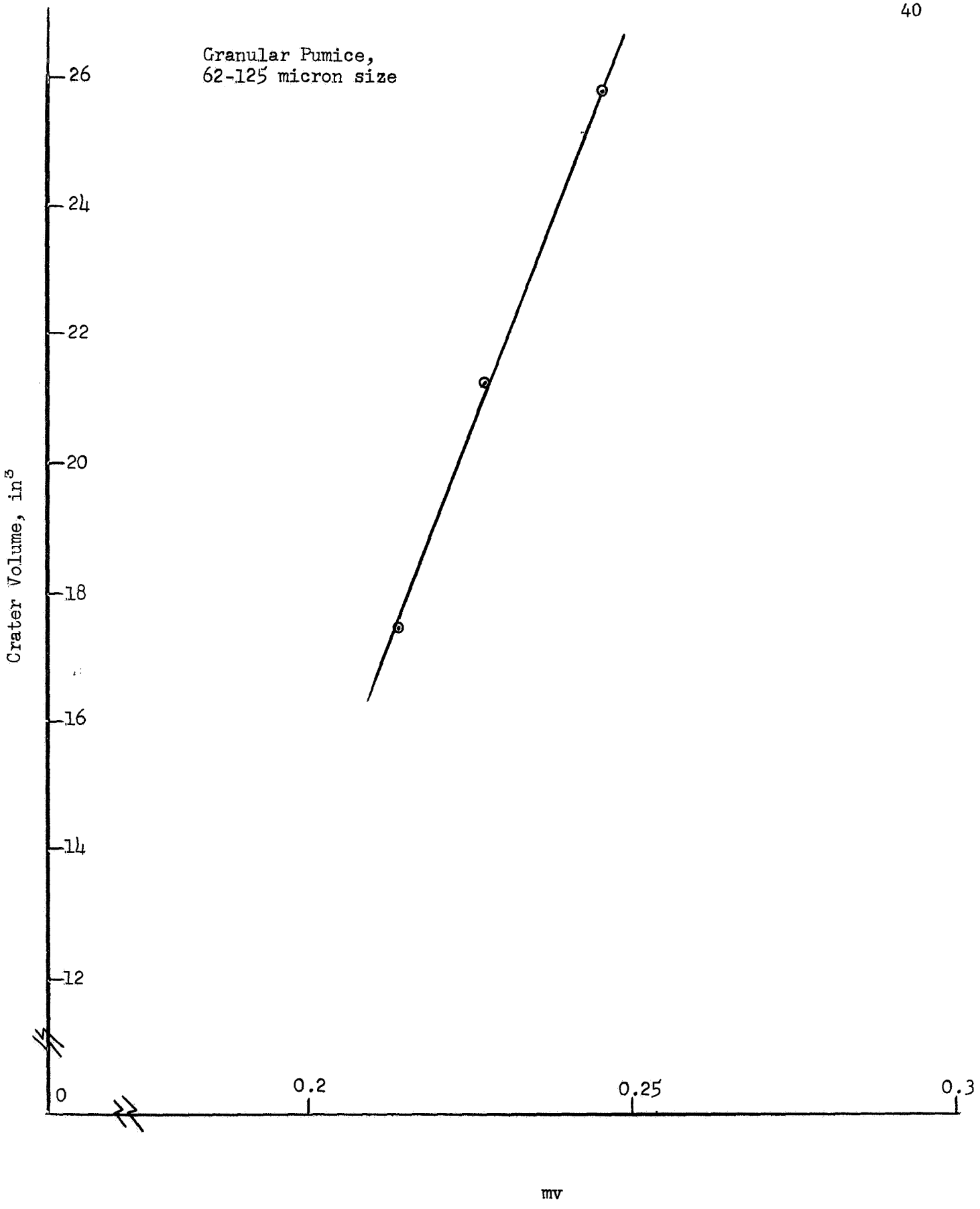
Granular Pumice,
62-125 micron size
26
24
22
20
18
16
14
12
Crater Volume, in³
0
0.2
0.25
0.3
mv

Fig. 4

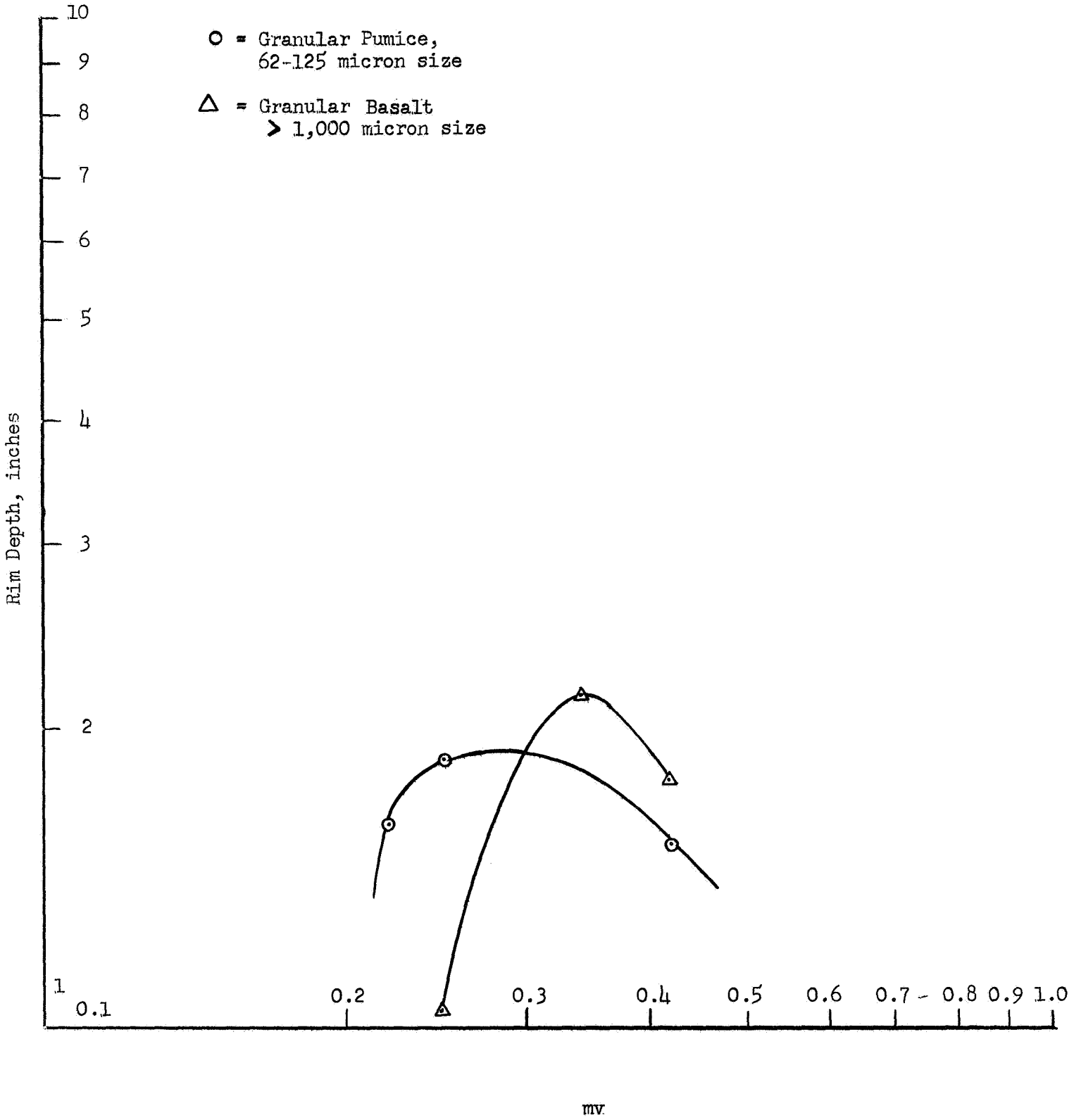
O = Granular Pumice, 62-125 micron size
△ = Granular Basalt > 1,000 micron size
Rim Depth, inches
10
9
8
7
6
5
4
3
2
1
0.1
0.2
0.3
0.4
0.5
0.6
0.7
0.8
0.9
1.0
mv

Fig. 5

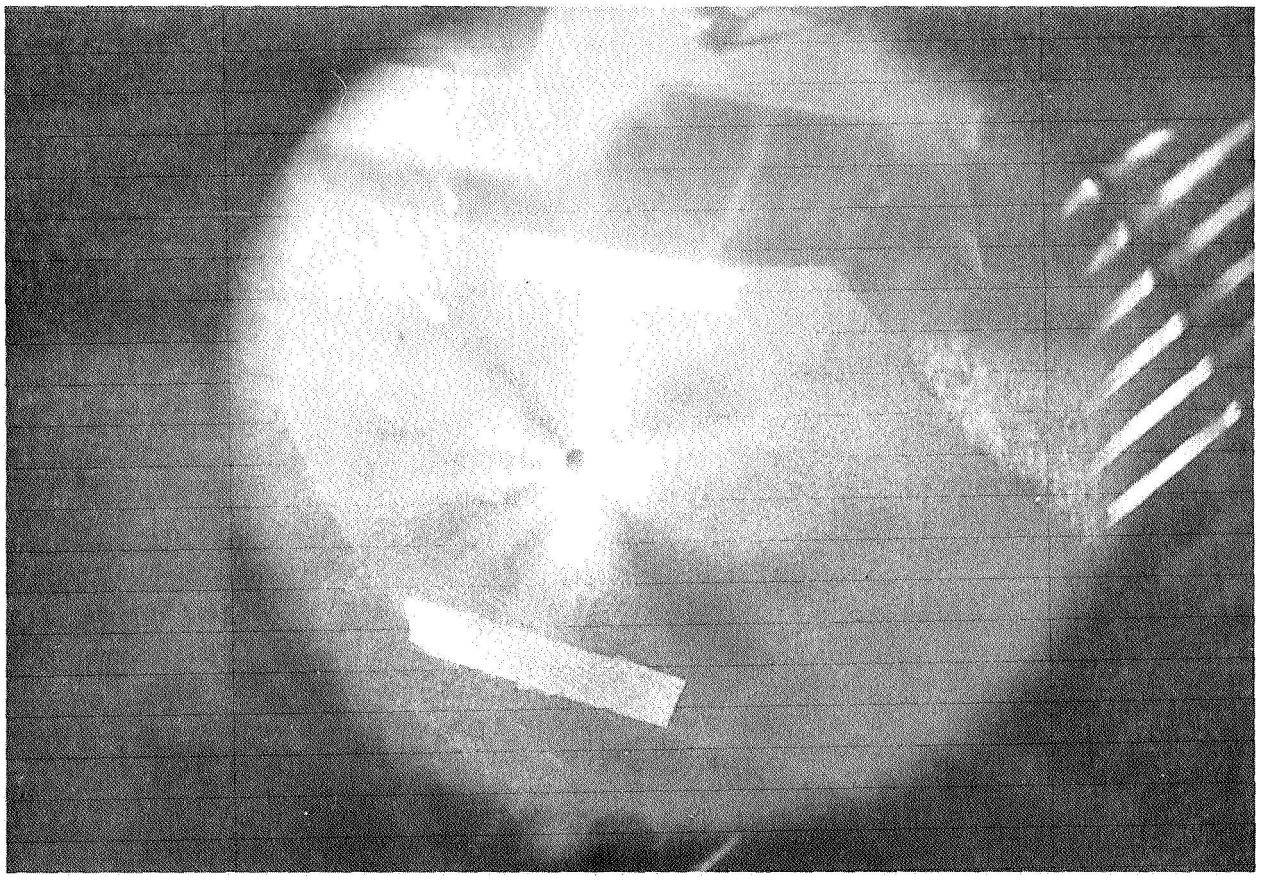

Impact photograph in solid basalt
140 micro-seconds after impact

Fig. 6

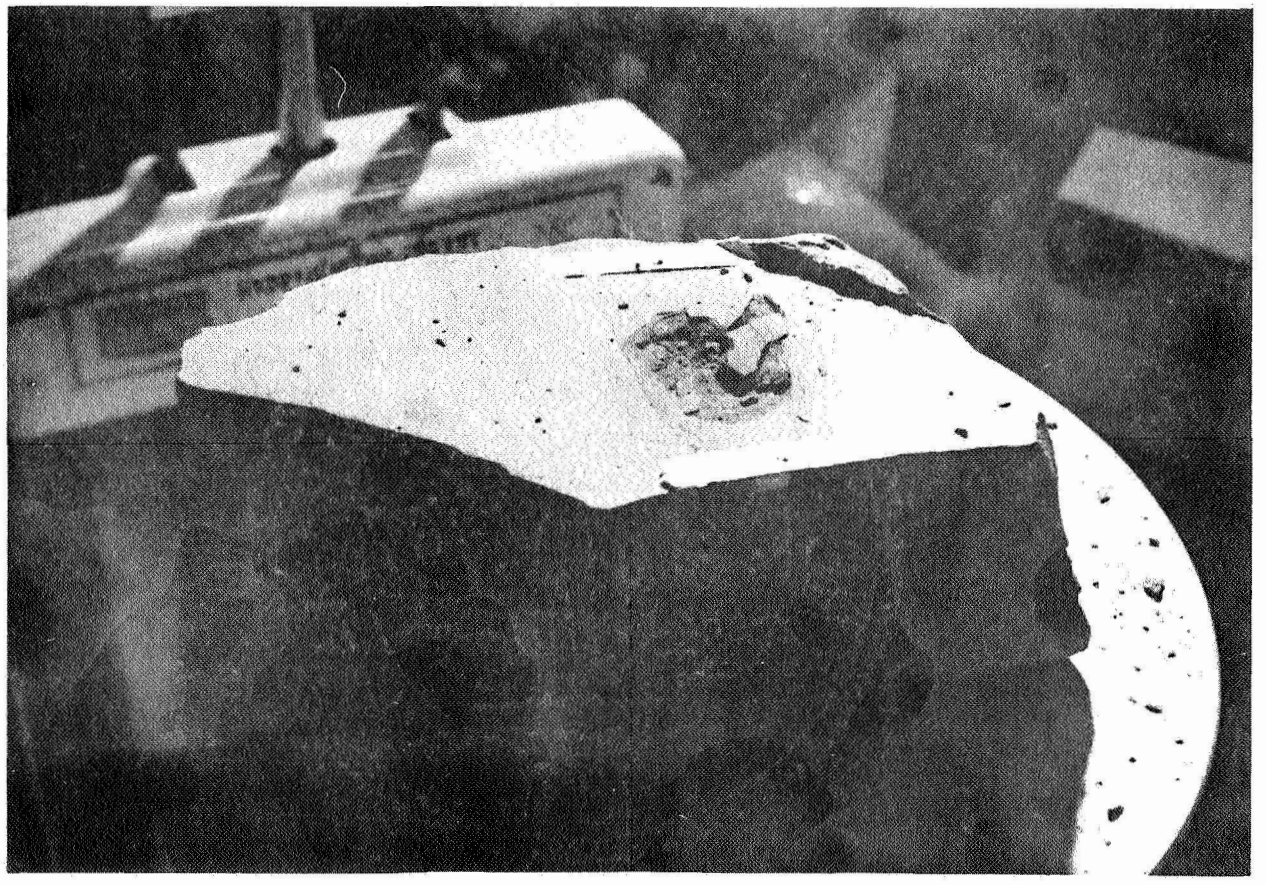

Typical crater in solid basalt

Fig. 7

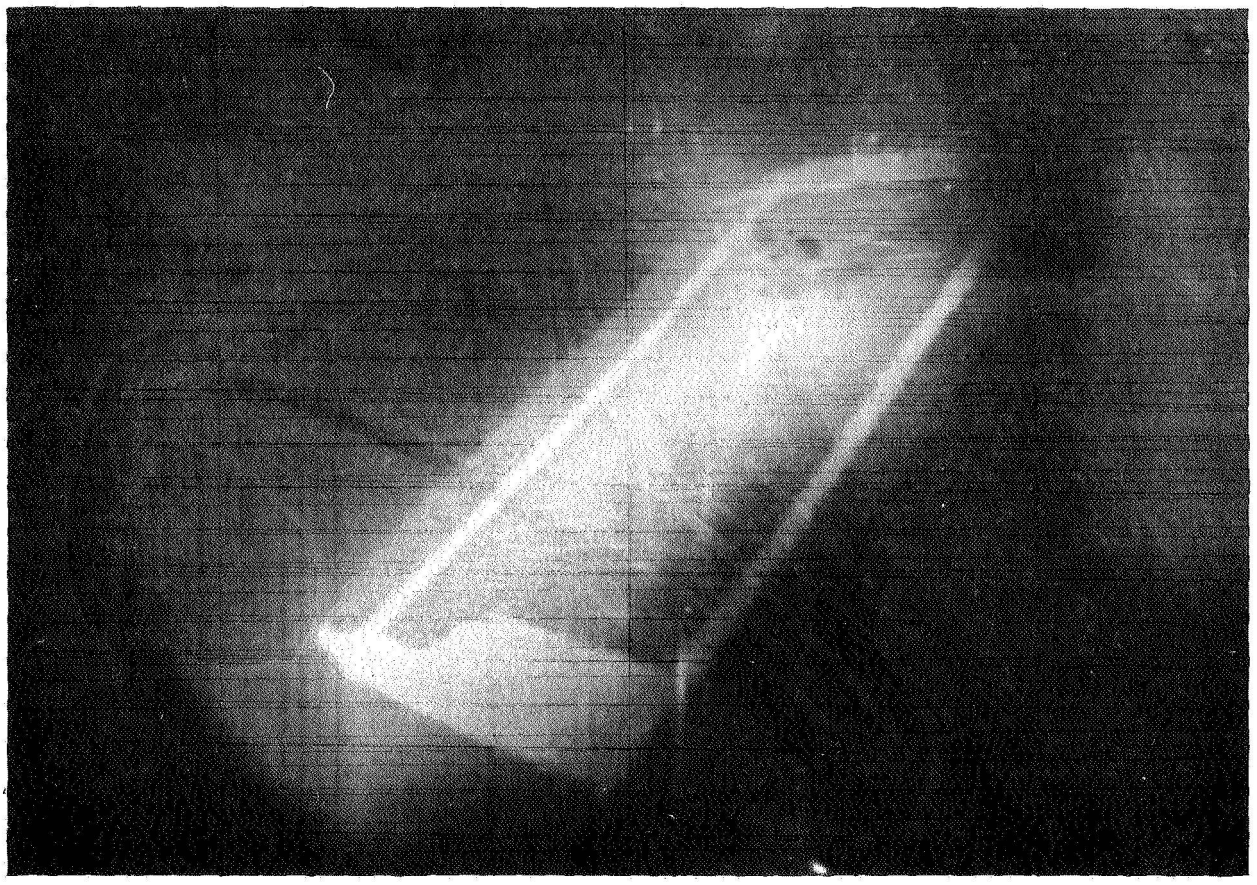

Impact photograph in solid basalt at 45 degree orientation. 1.5 milli-seconds after impact.

Fig. 8

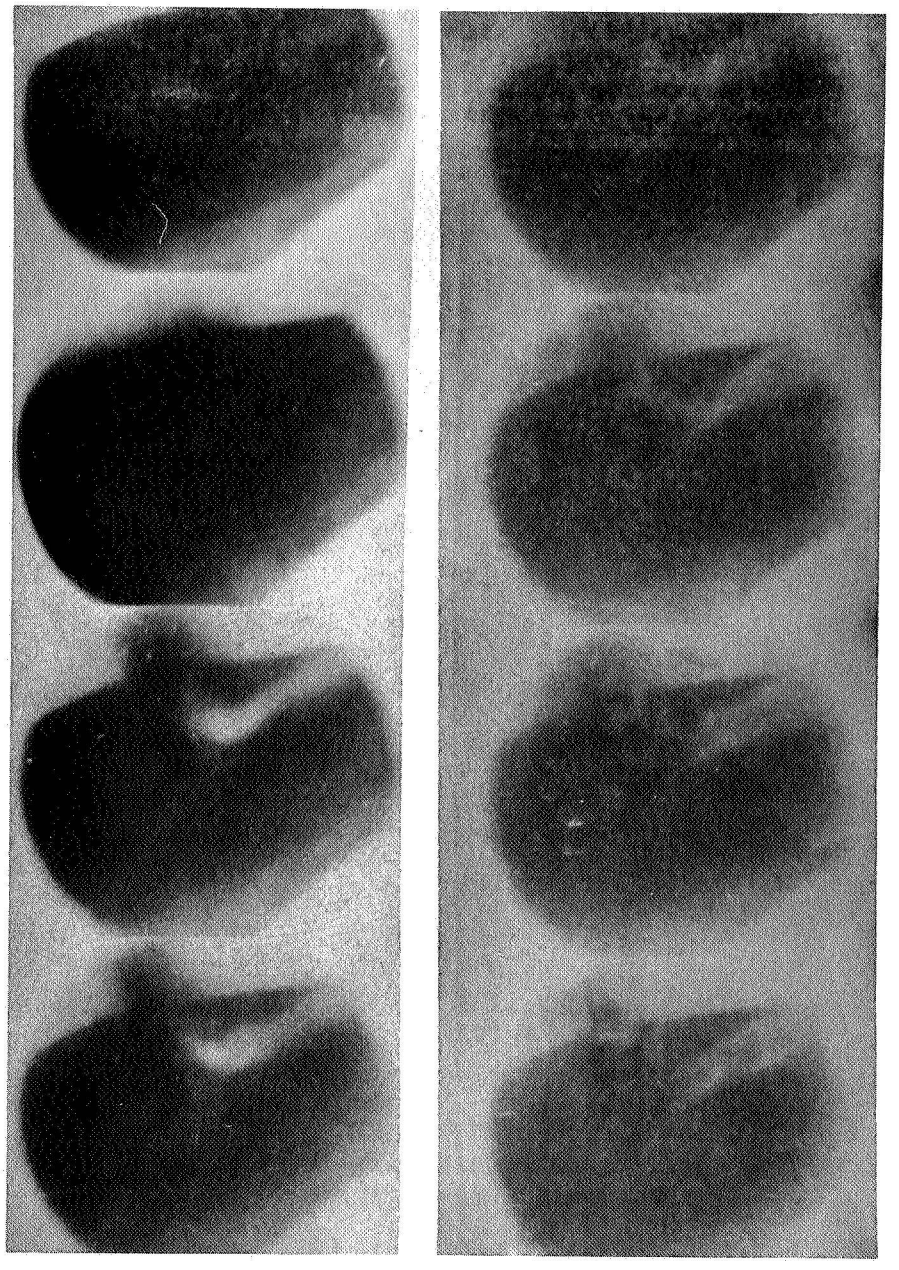

Impact sequence in solid basalt-
from 16mm motion picture film.
Frame rate 5,000 pps

Fig. 9

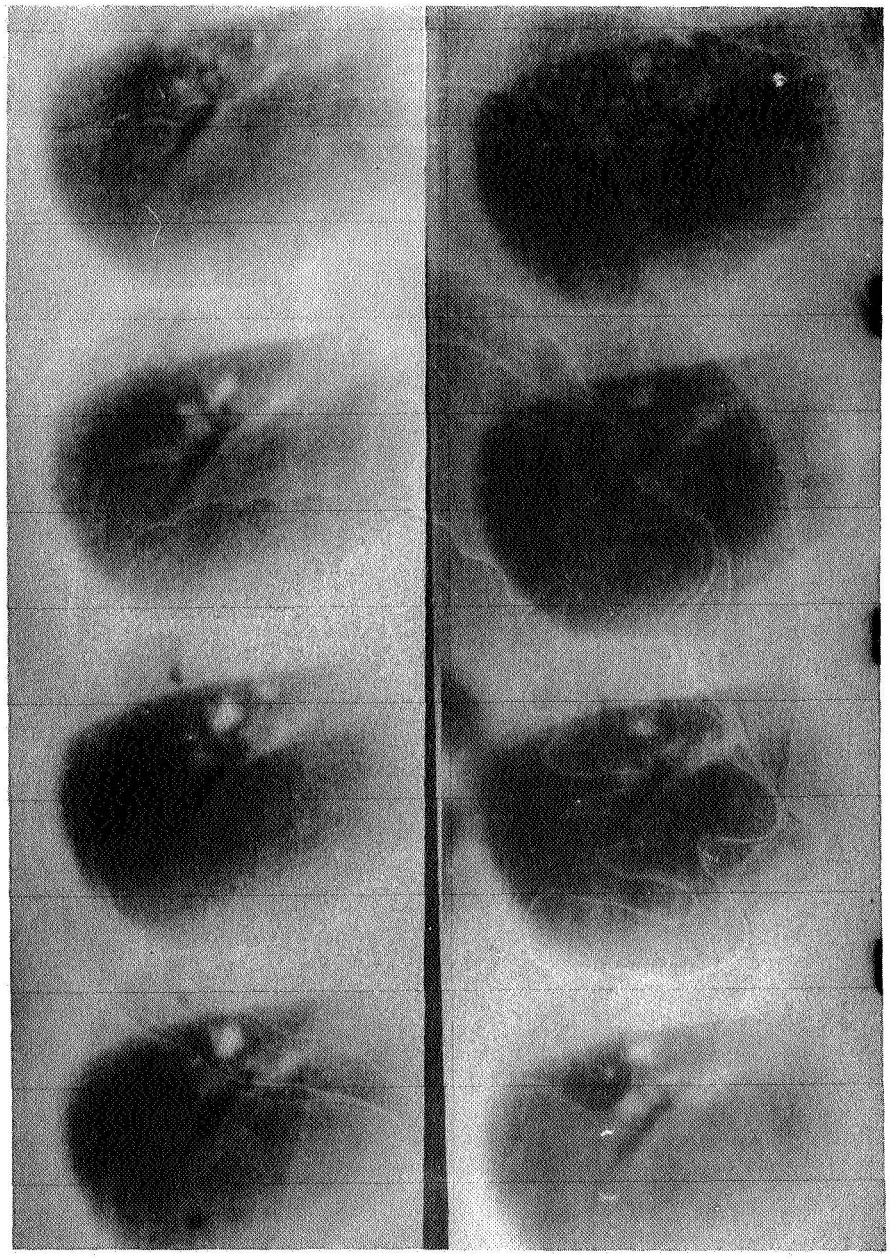

Continuation of impact sequence in
solid basalt at 45 degree orientation.

Fig. 10

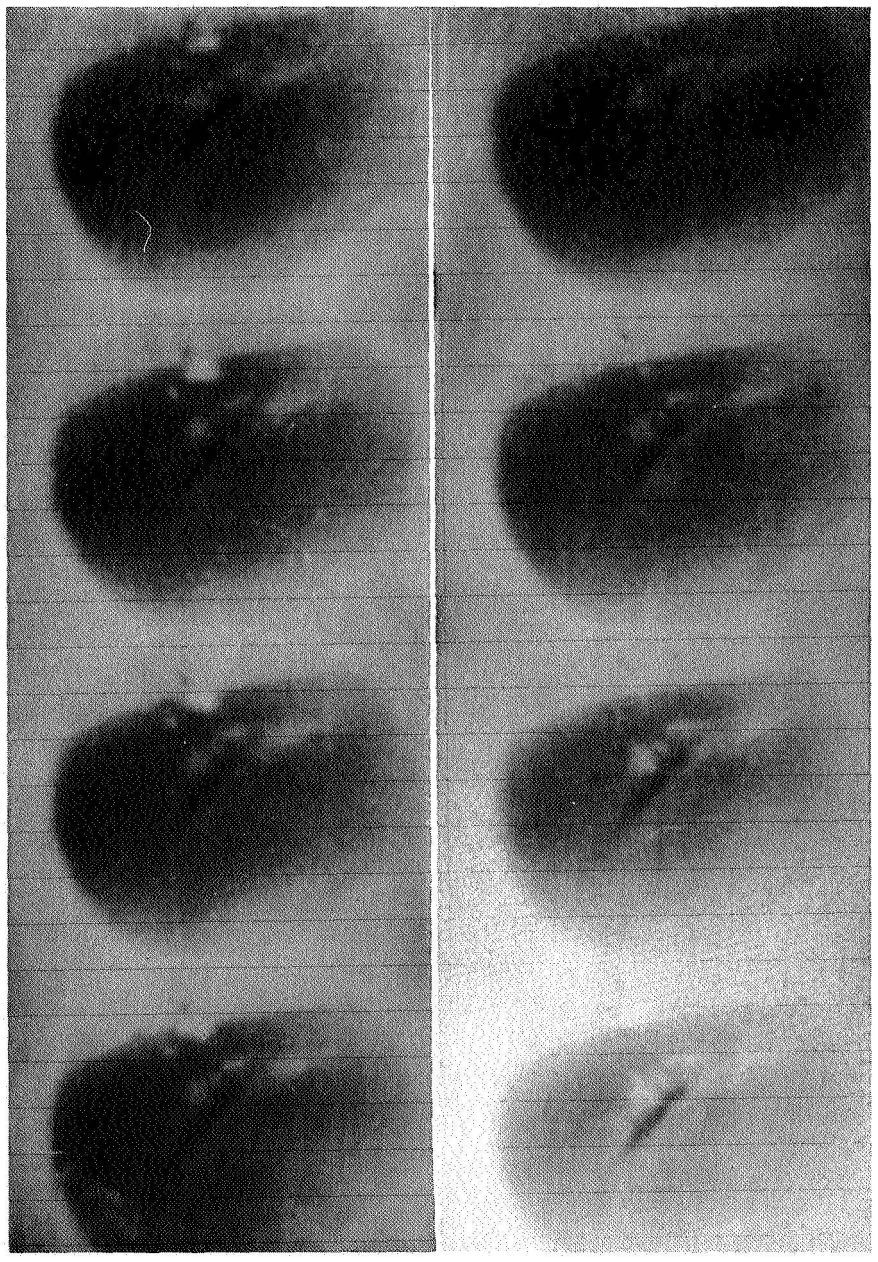

Continuation of impact sequence in
solid basalt at 45 degree orientation.

Fig. 11

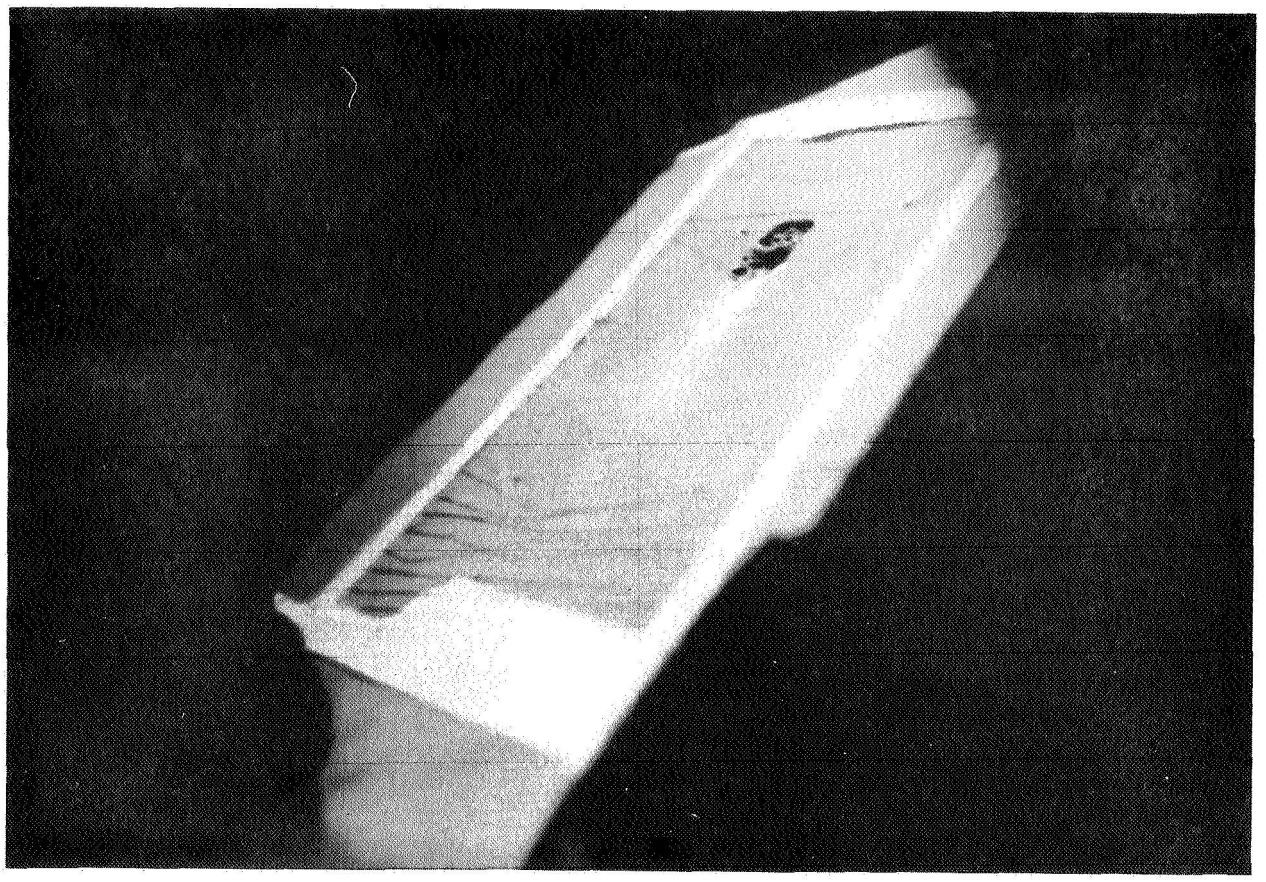

Typical crater in solid basalt
at 45 degree orientation.

Fig. 12

Impact sequence in vesicular basalt.
2.22 milli-seconds after impact.

Fig. 13

Impact sequence in vesicular basalt.
3.65 milli-seconds after impact.

Fig. 14

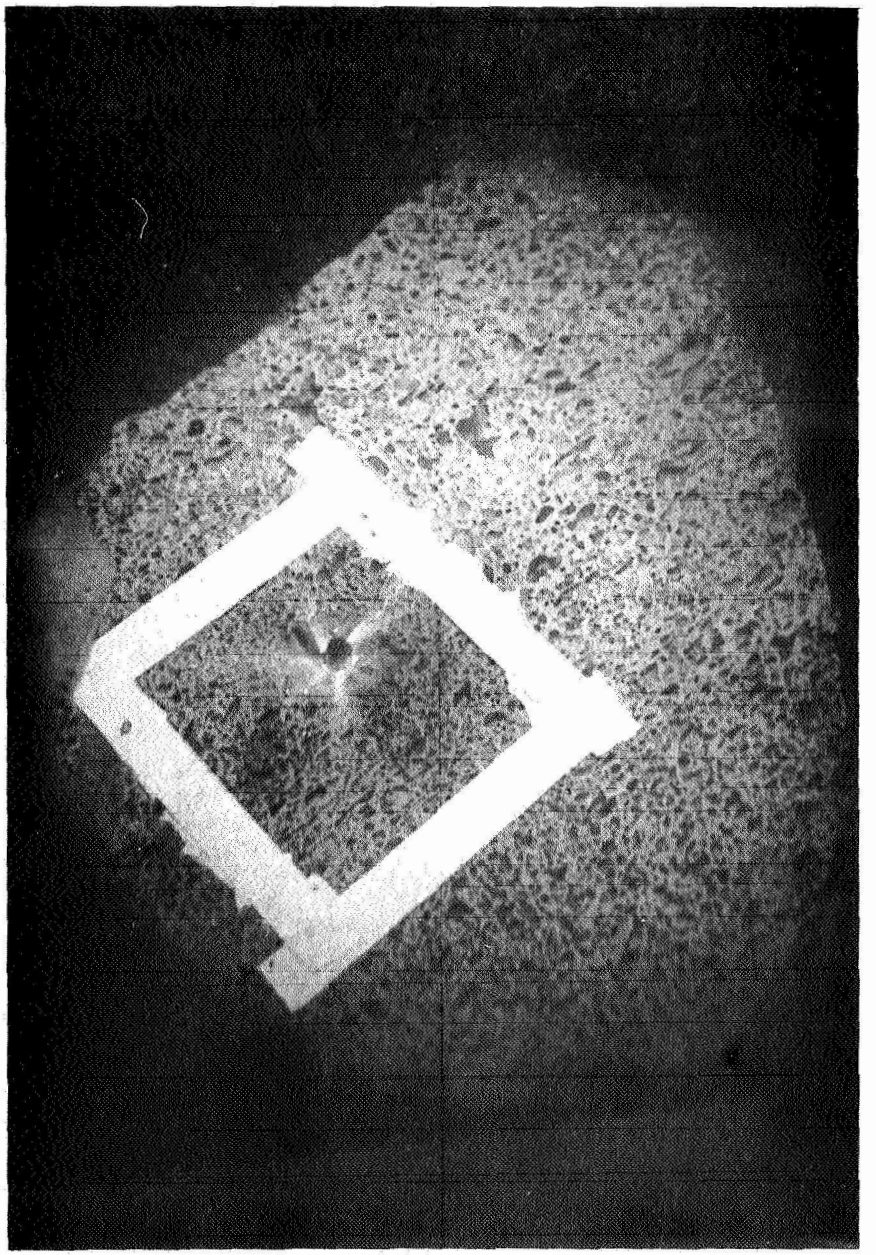

Impact sequence in vesicular basalt.
4.20 milli-seconds after impact.

Fig. 15

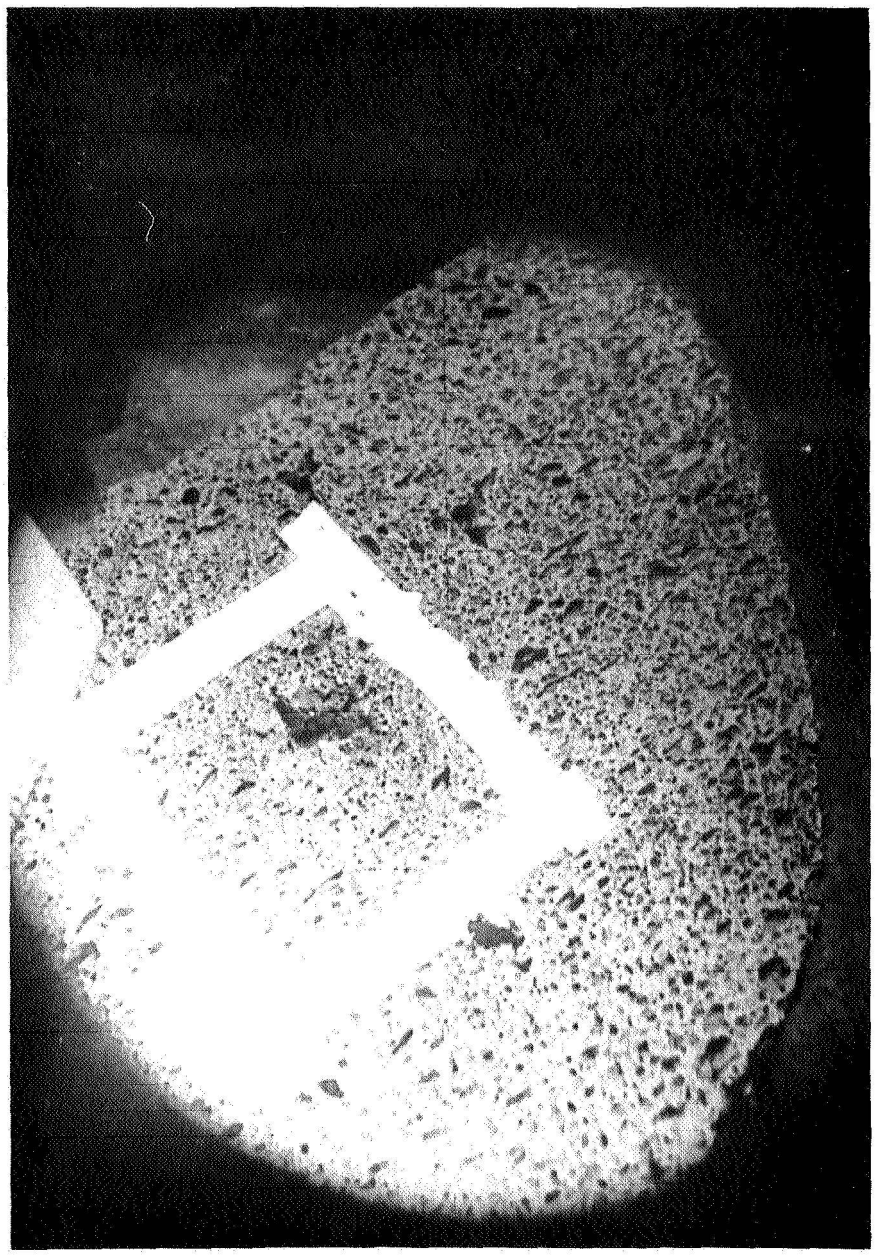

Impact sequence in vesicular basalt.
Typical crater after impact.

Fig. 16

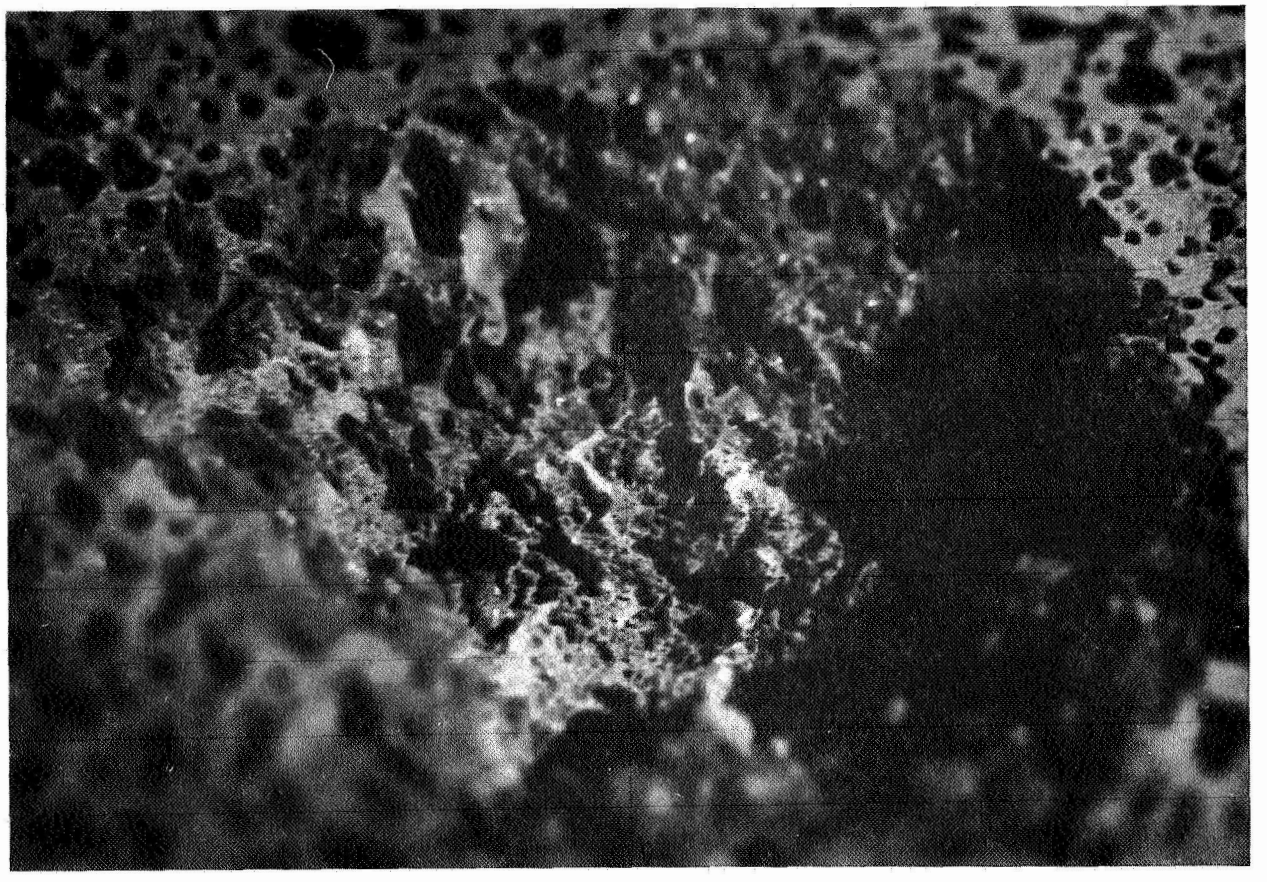

Close-up of typical crater in vesicular basalt

Fig. 17

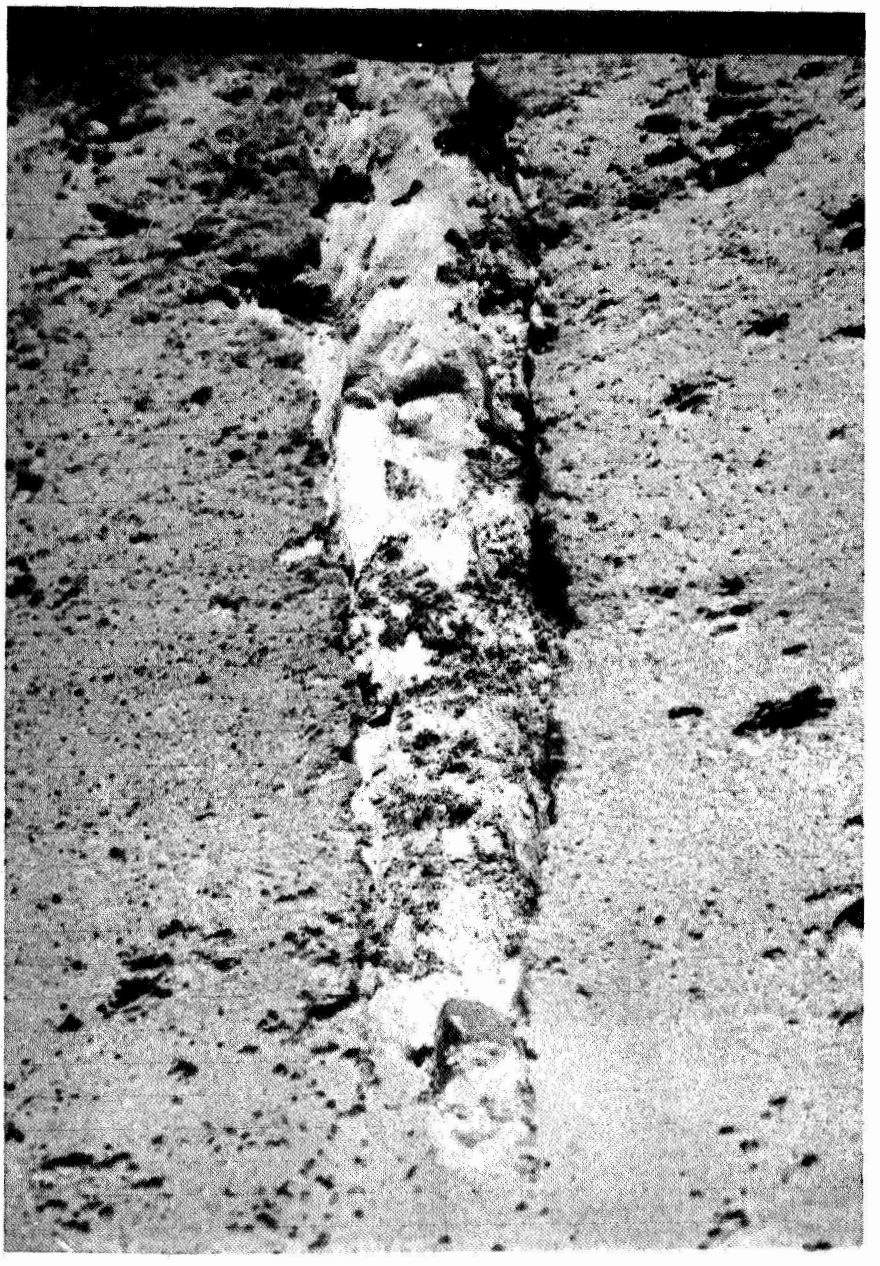

Sequence of crater development with increasing density in solid pumice. Least dense sample produces deep, narrow burrow.

Fig. 18

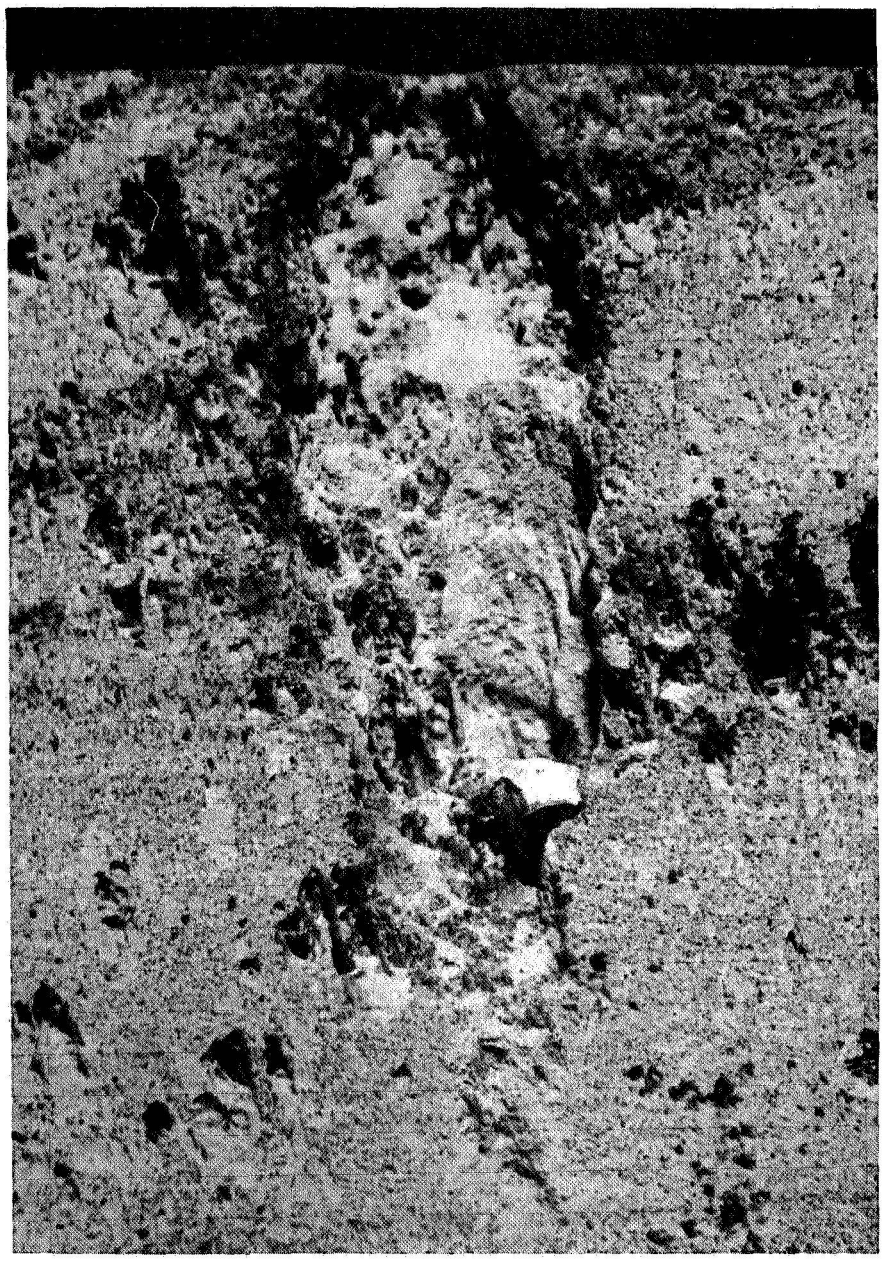

Sequence of crater development with increasing density in solid pumice. Denser sample produces fairly deep, elliptical burrow.

Fig. 19

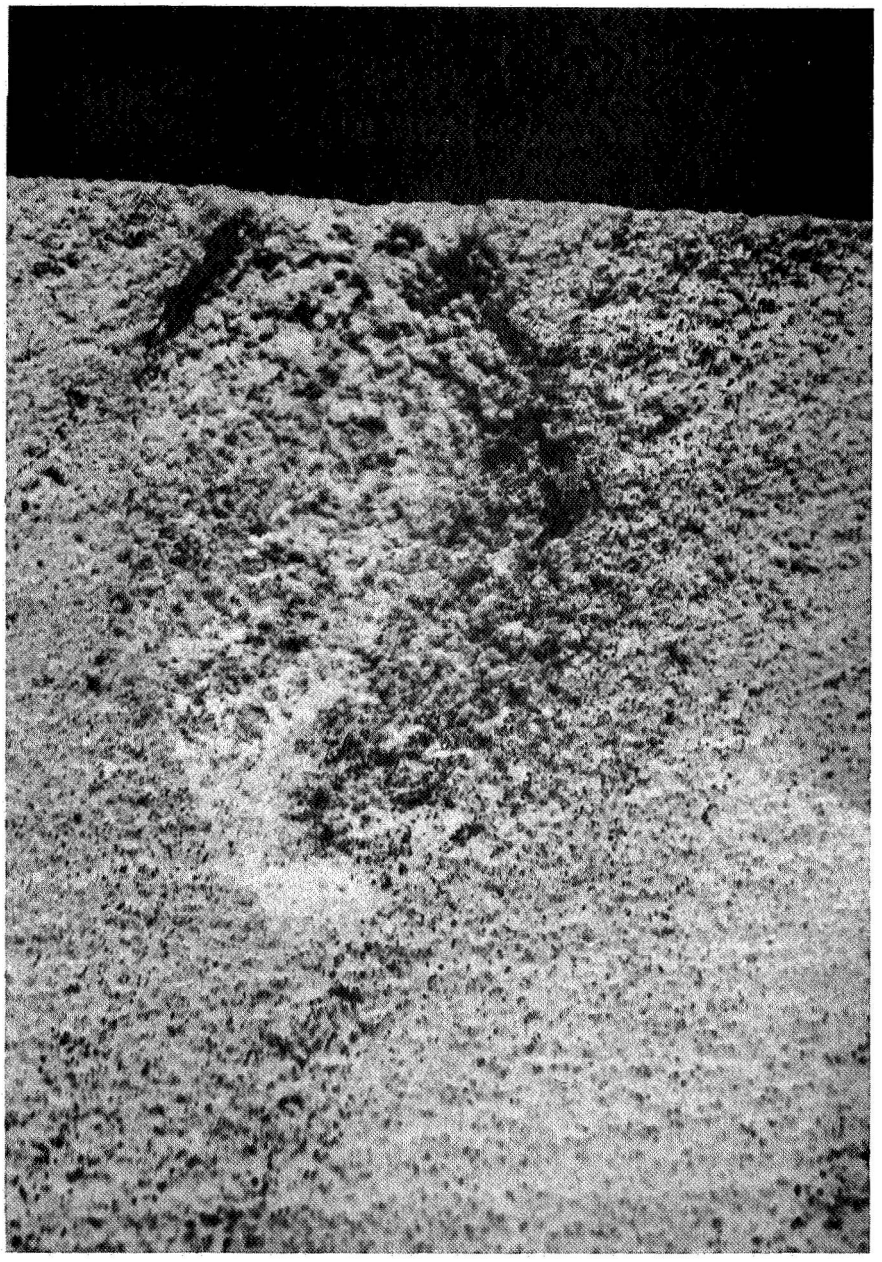

Sequence of crater development with increasing density in solid pumice. Denser sample produces shallow, elliptic crater with small entry hole.

Fig. 20

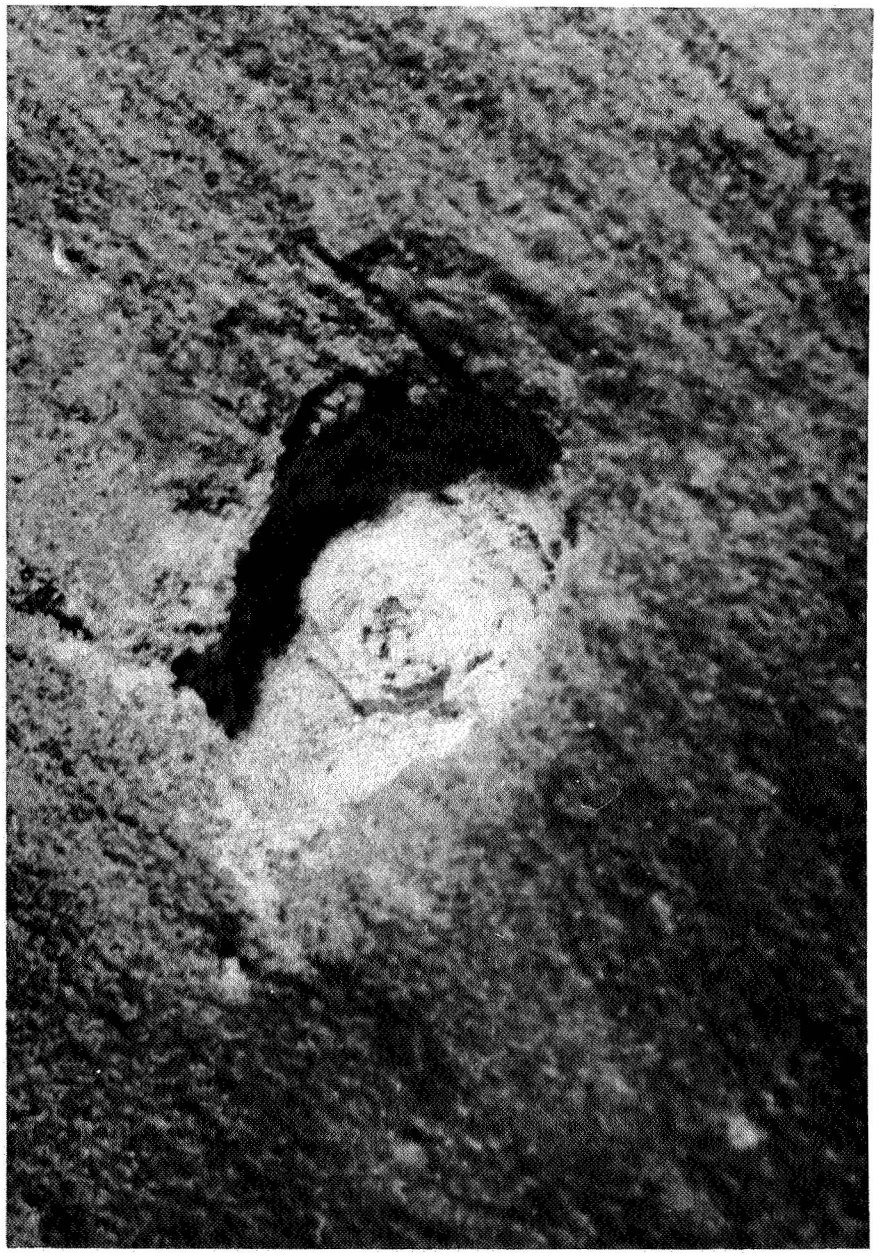

Sequence of crater development with increasing density in solid pumice. Densest sample produces shallow, impact-shear type crater with central elevation.

Fig. 21

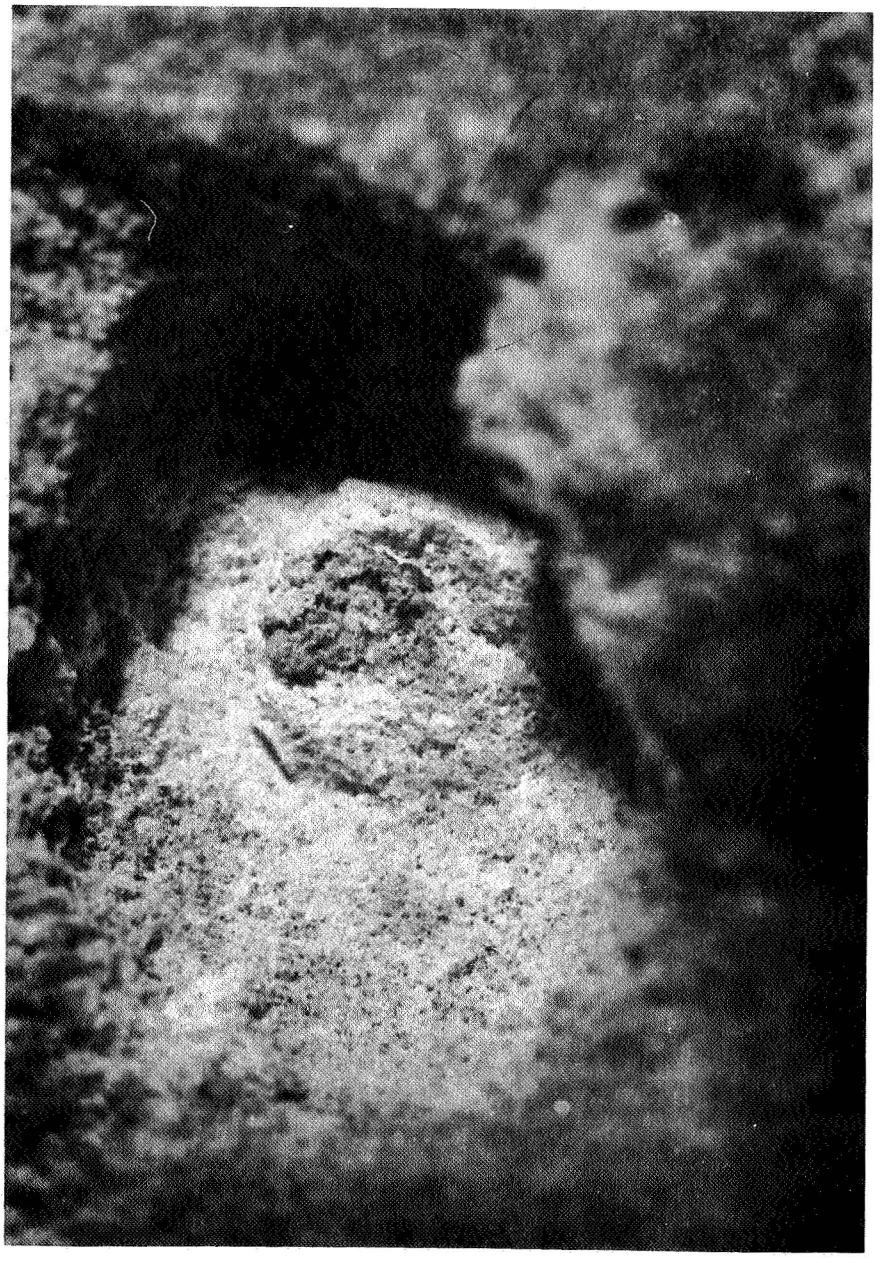

Close-up of central crater elevation
in solid pumice sample of densest type.

Fig. 22

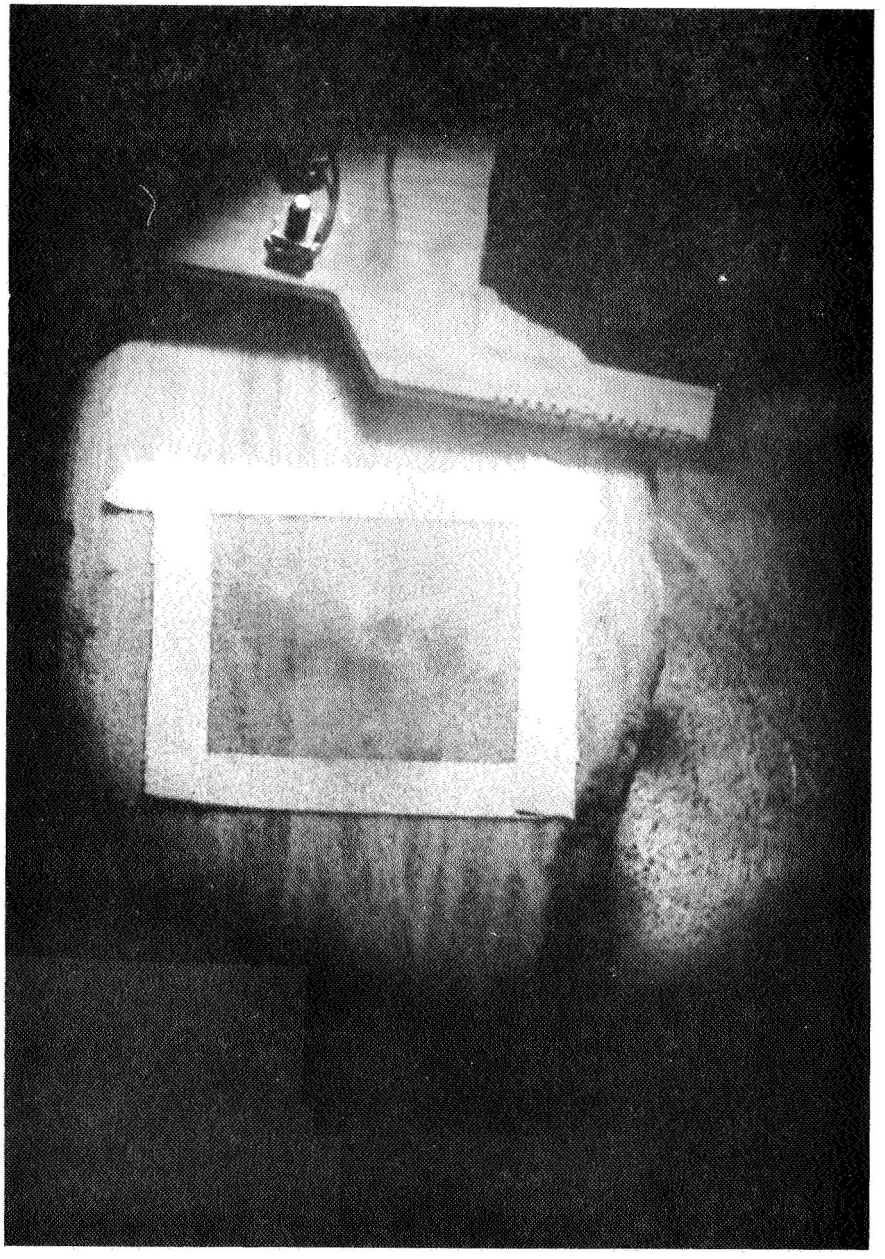

Impact photograph of solid pumice.
Sample of Fig. 20. 880 micro-seconds
after impact.

Fig. 23

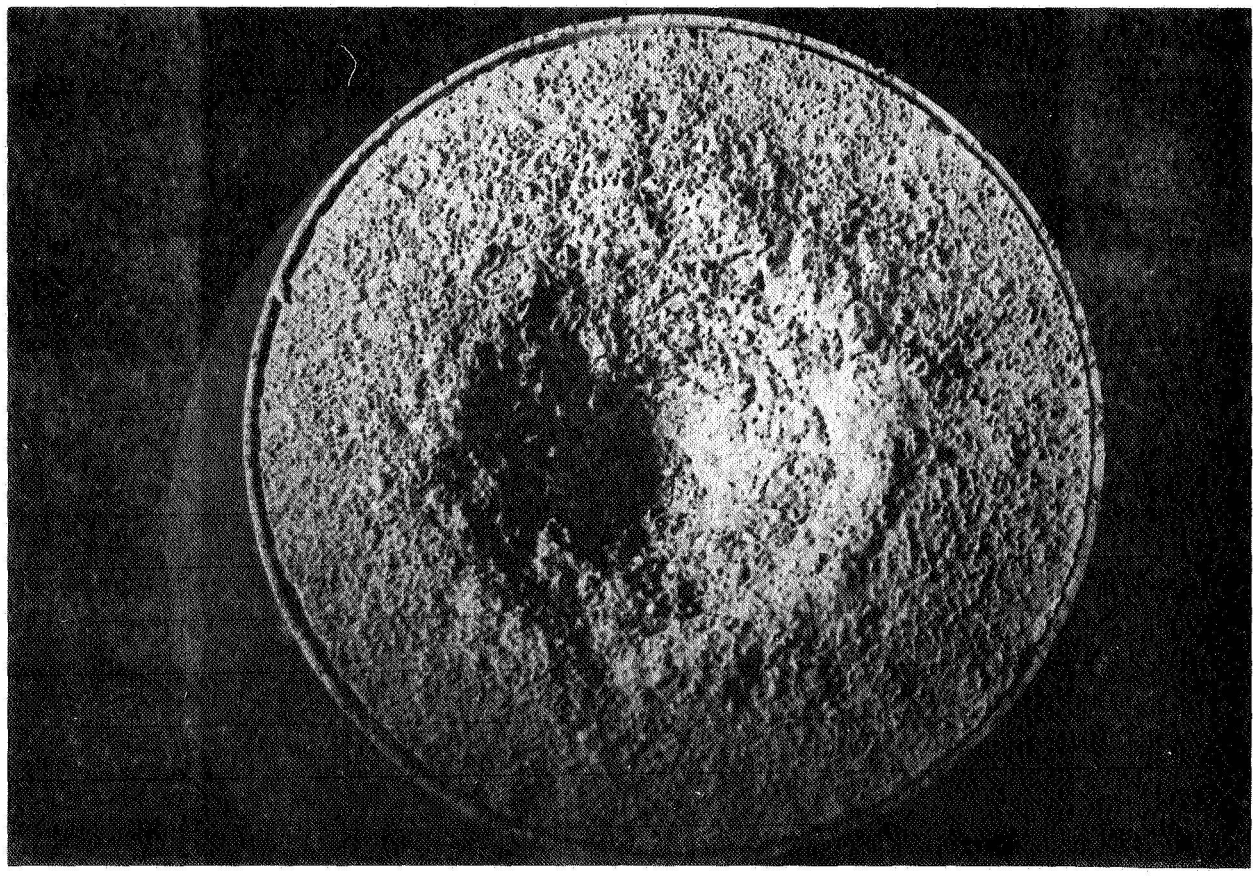

Vertical view of crater in granular basalt, 20-62 micron size.

Fig. 24

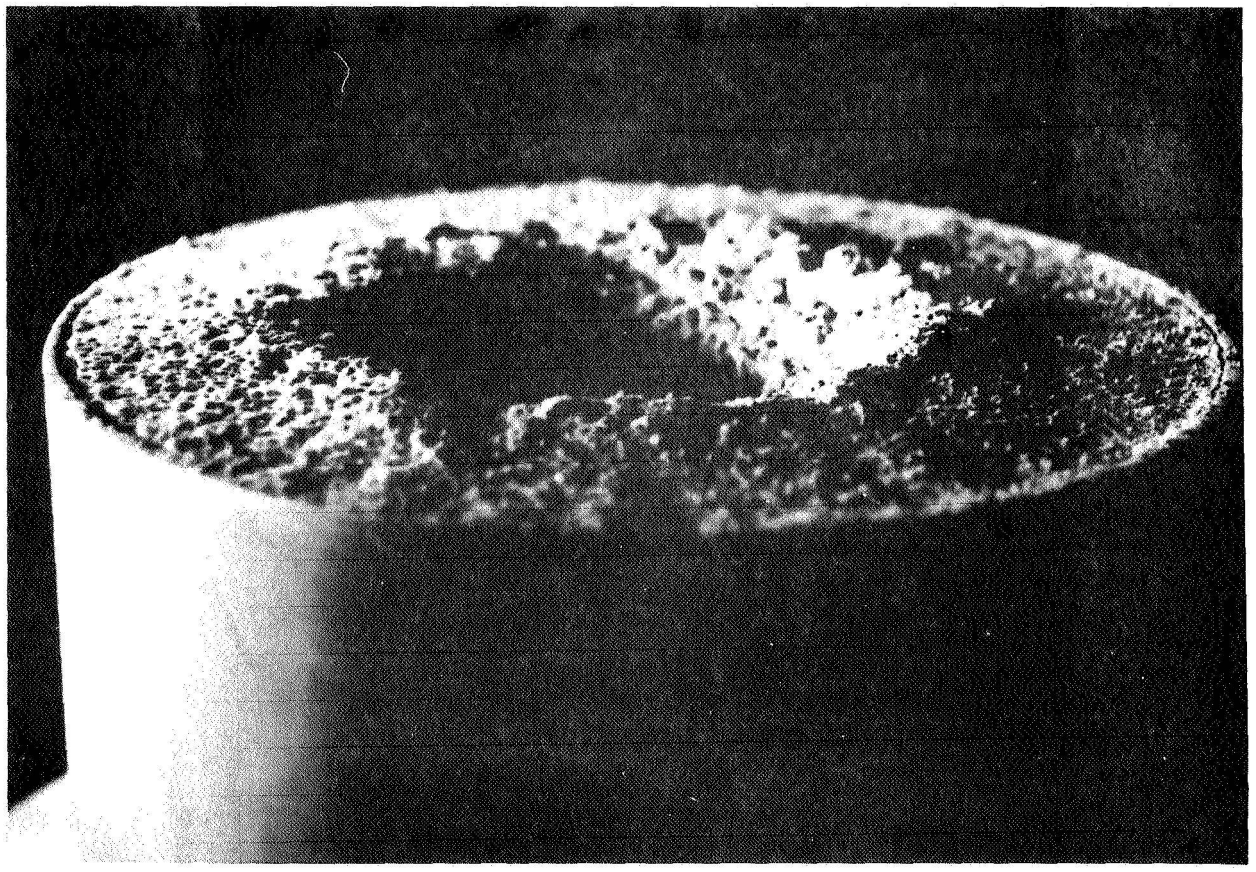

Horizontal view of crater in granular basalt, 20-62 micron size.

Fig. 25

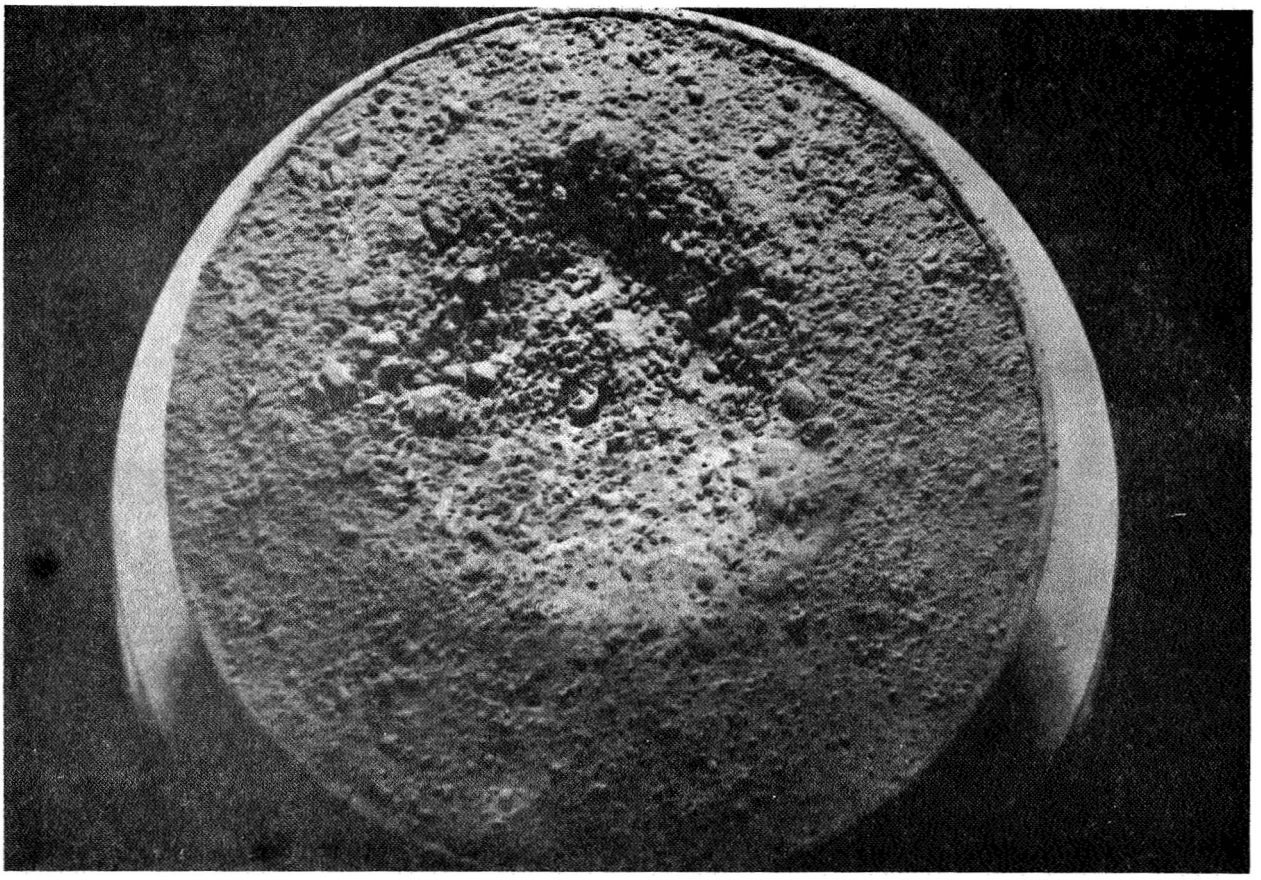

Vertical view of crater in granular basalt-62-125 micron size.

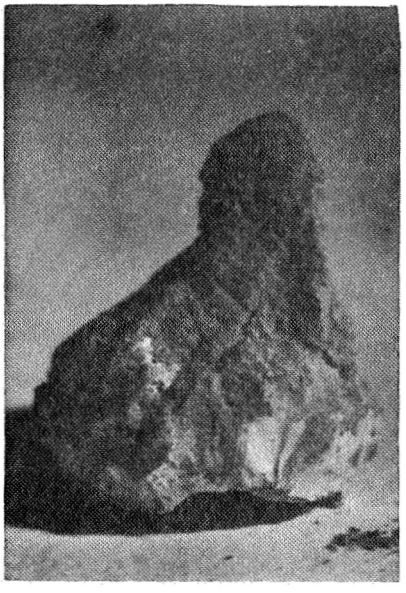

Close-up of projectile. Note cone of compacted material.

Fig. 26

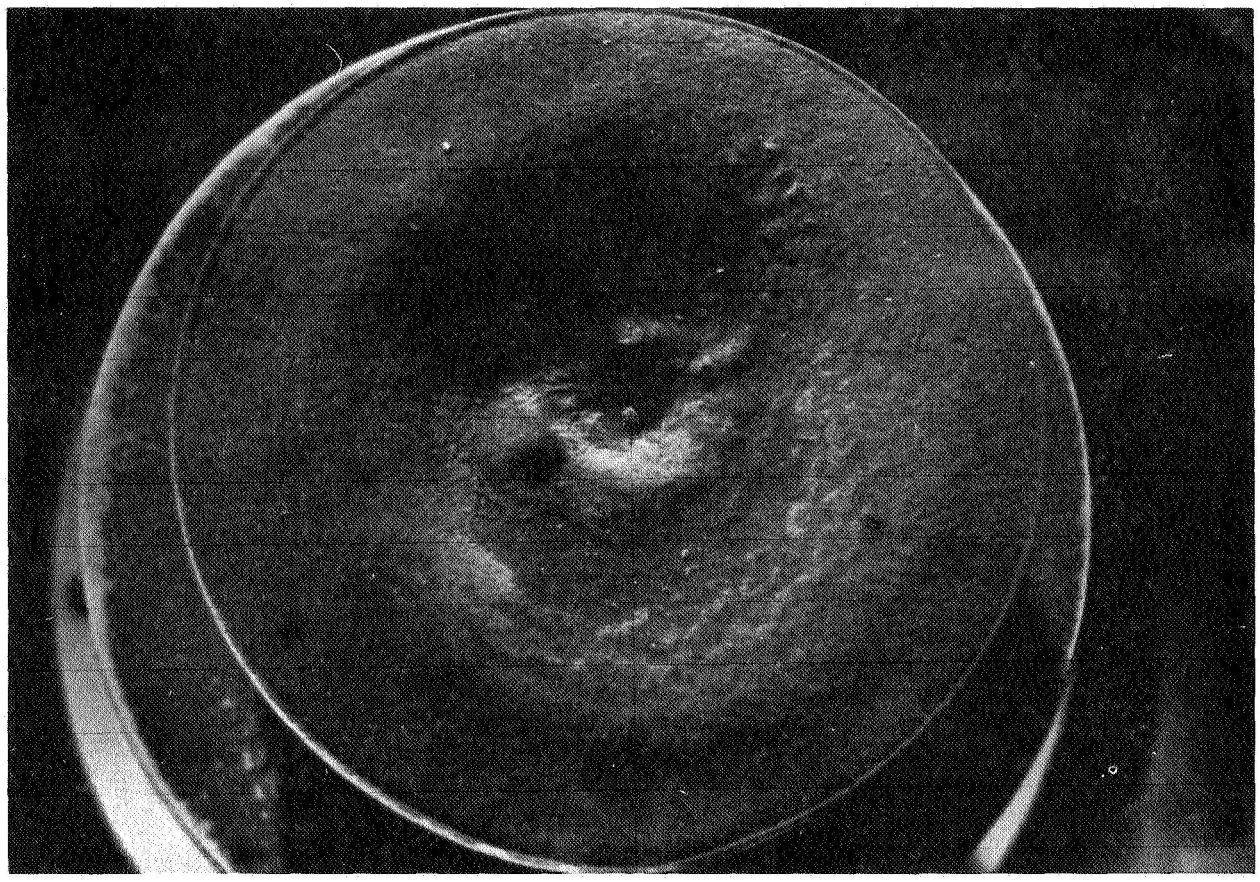

Vertical view of crater in granular basalt, 125-250 micron size.

Fig. 27

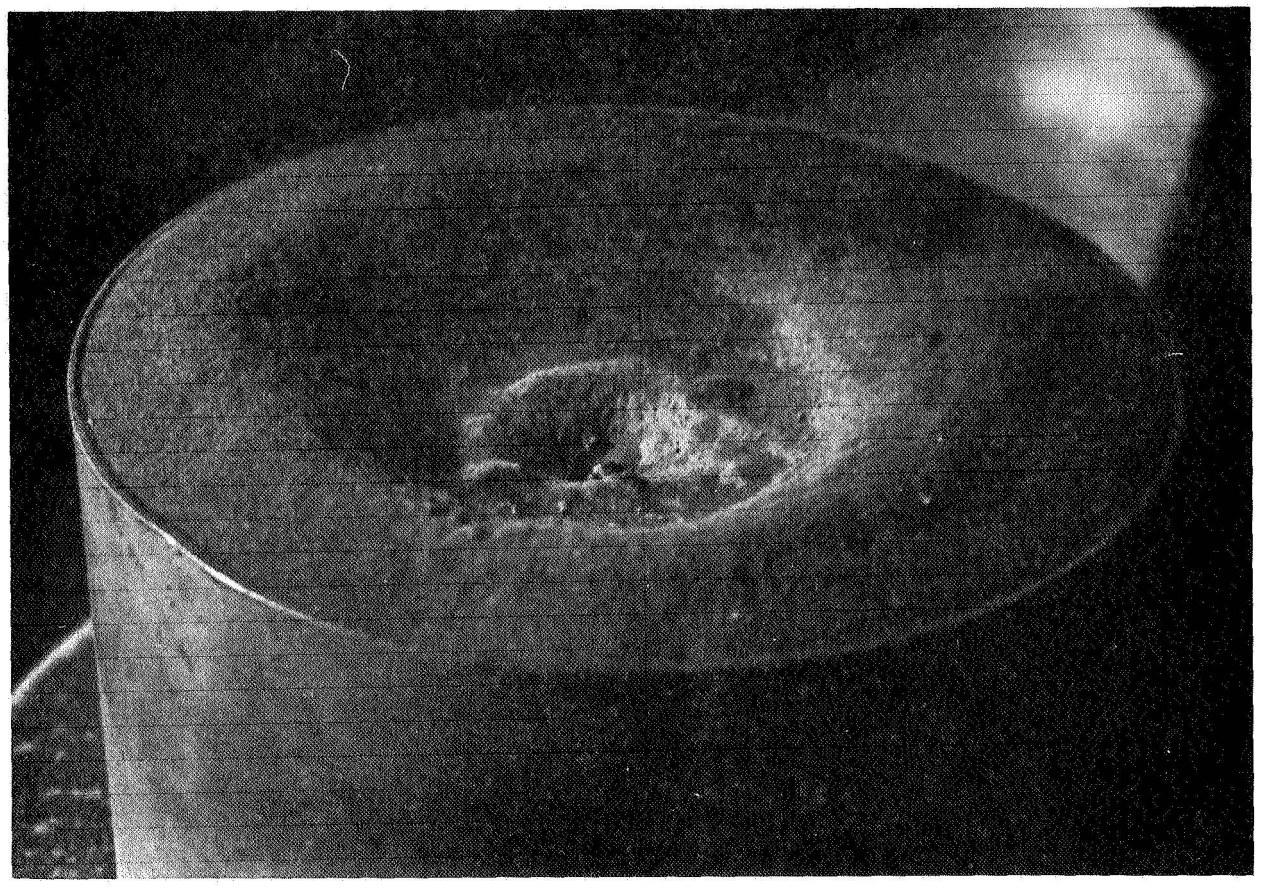

Three-quarter view of crater in
granular basalt, 125-250 micron size.

Fig. 28

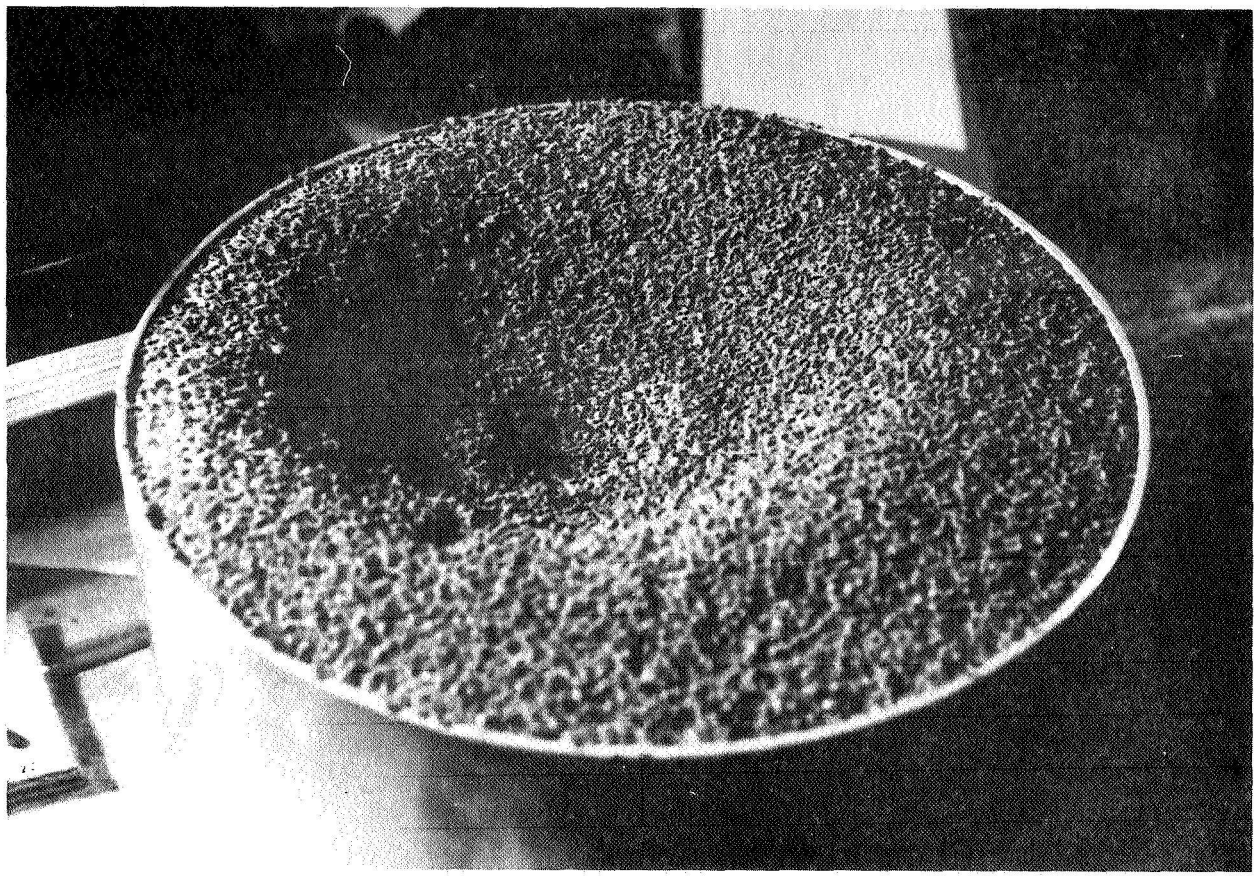

Crater in granular basalt,
500-1,000 micron size

Fig. 29

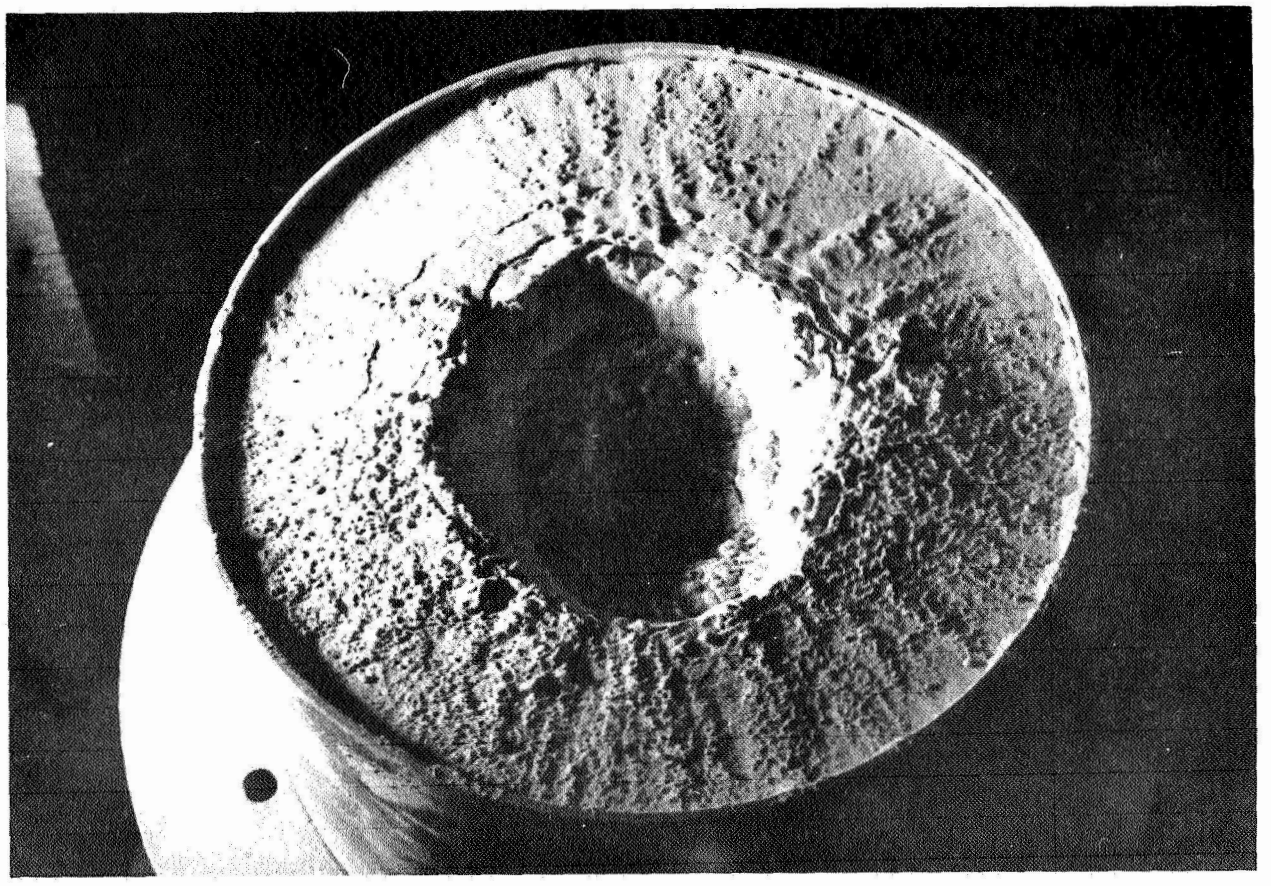

Crater in granular pumice,
10-37 micron size.

Fig. 30

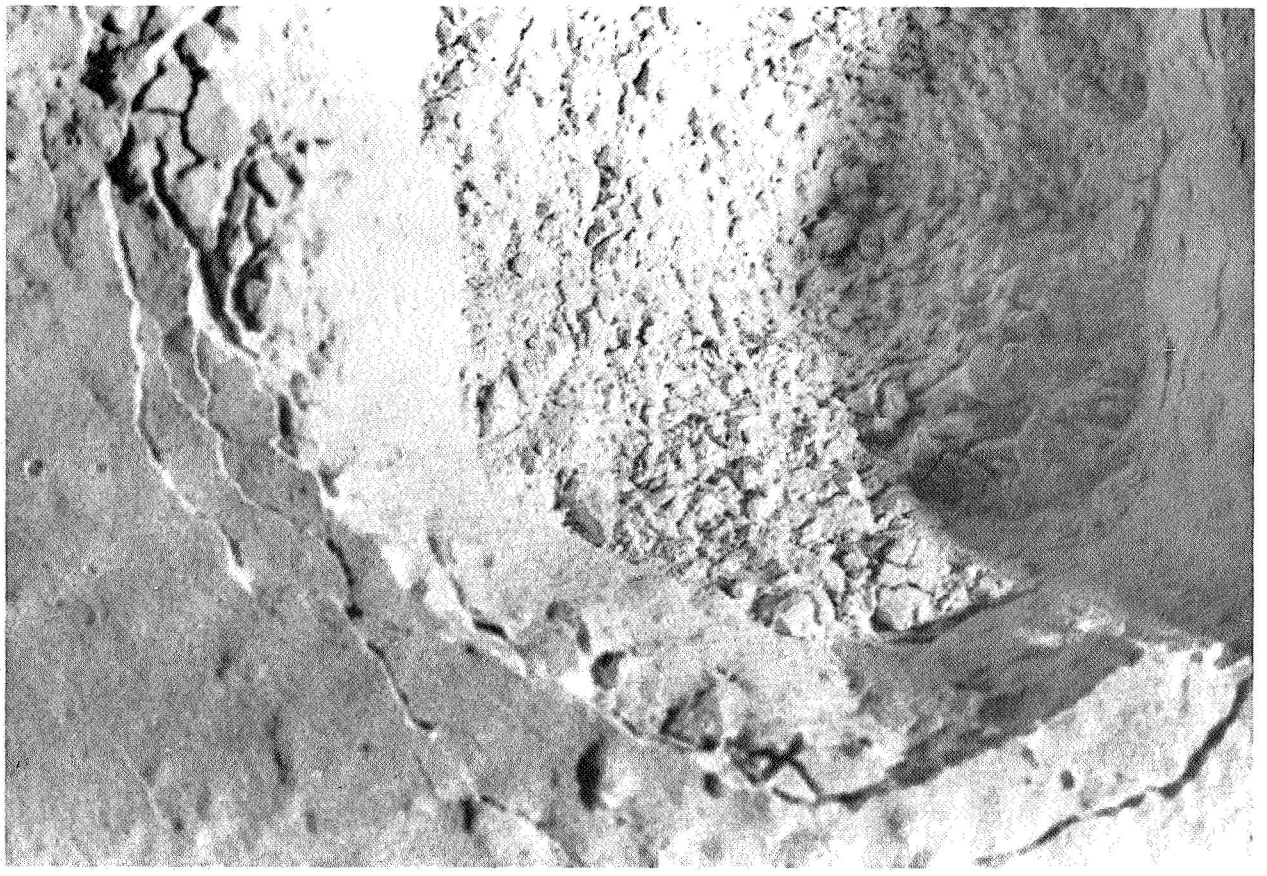

Close-up of crater rim in granular pumice, 10-37 micron size.

Fig. 31

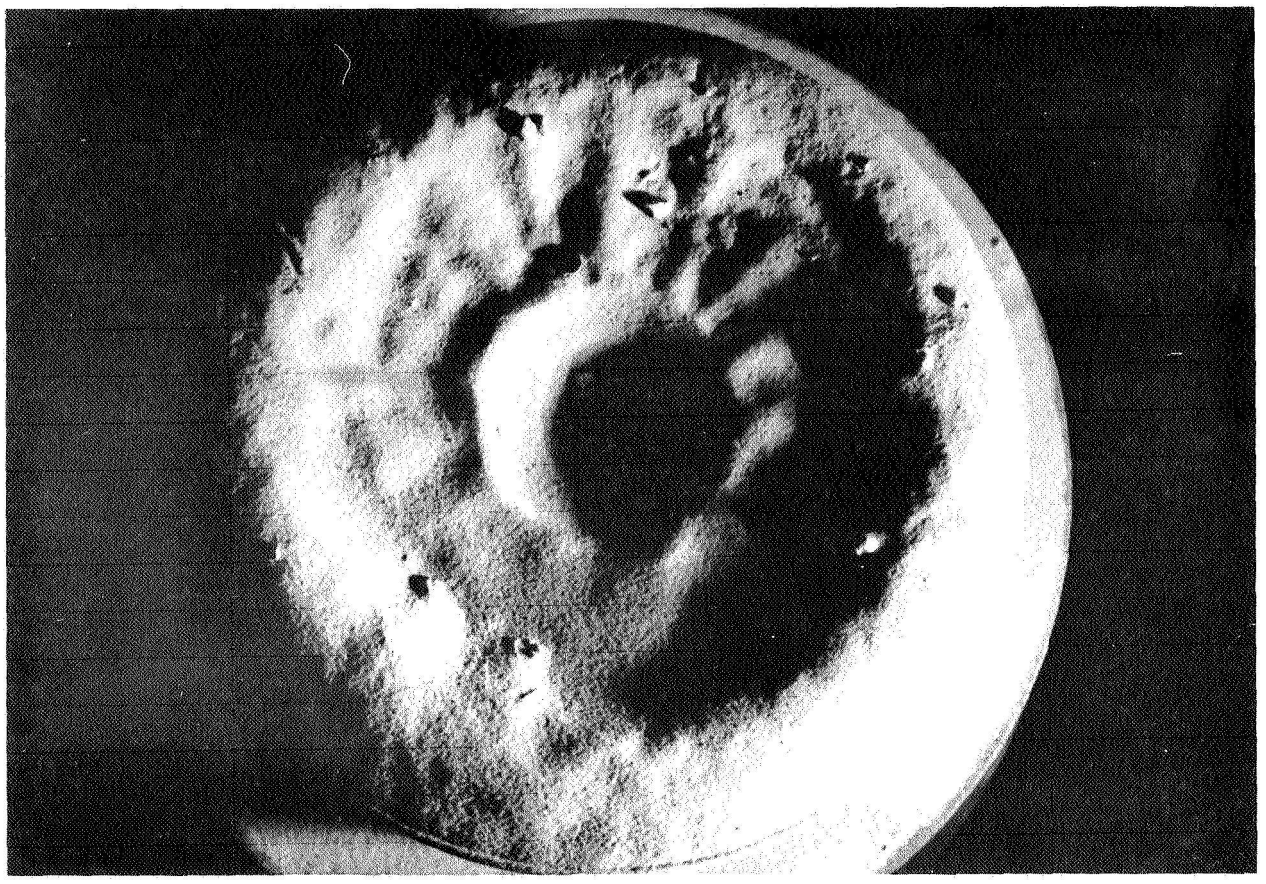

Vertical view of crater in granular pumice, 62-125 micron size. Low energy impact.

Fig. 32

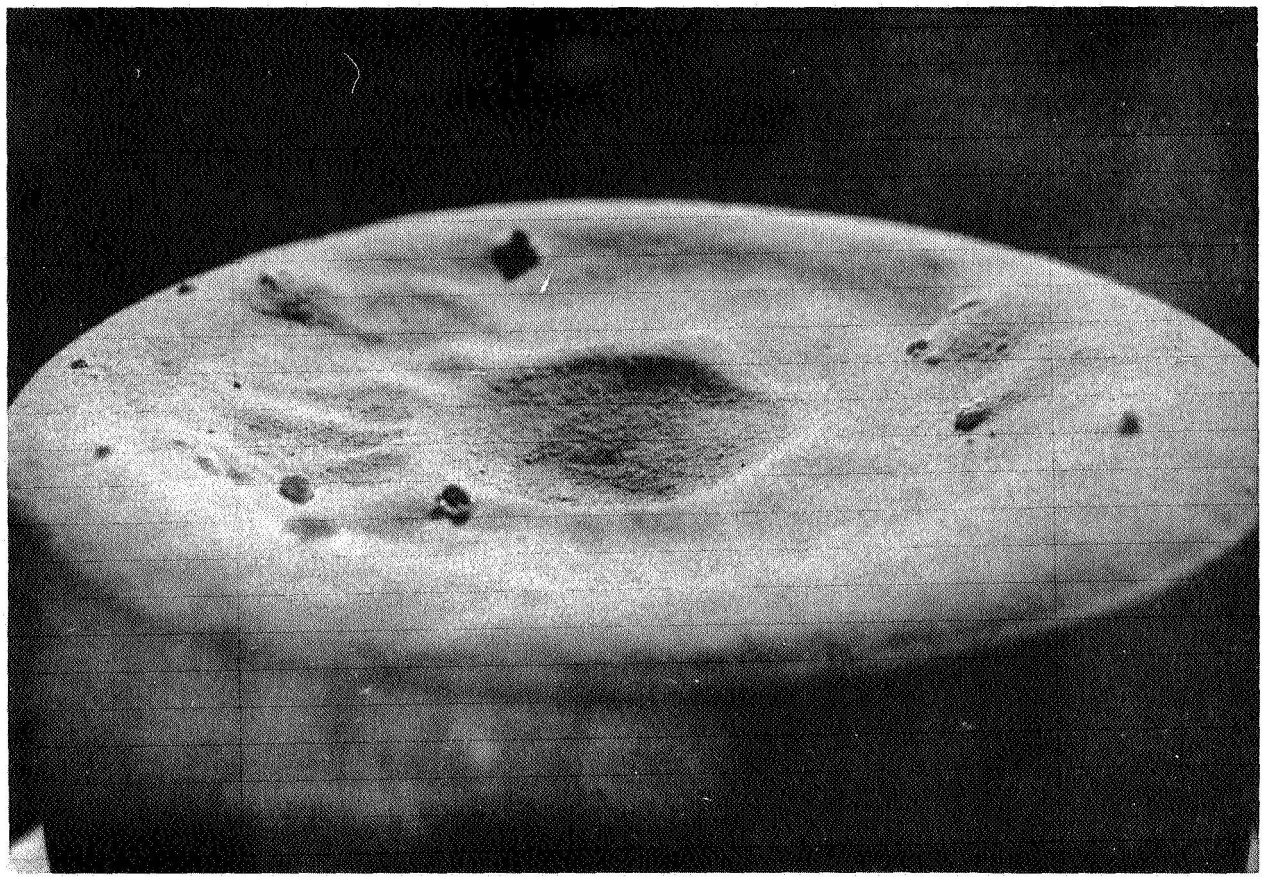

Crater in granular pumice, 62-125 micron size. Low energy impact.

Fig. 33

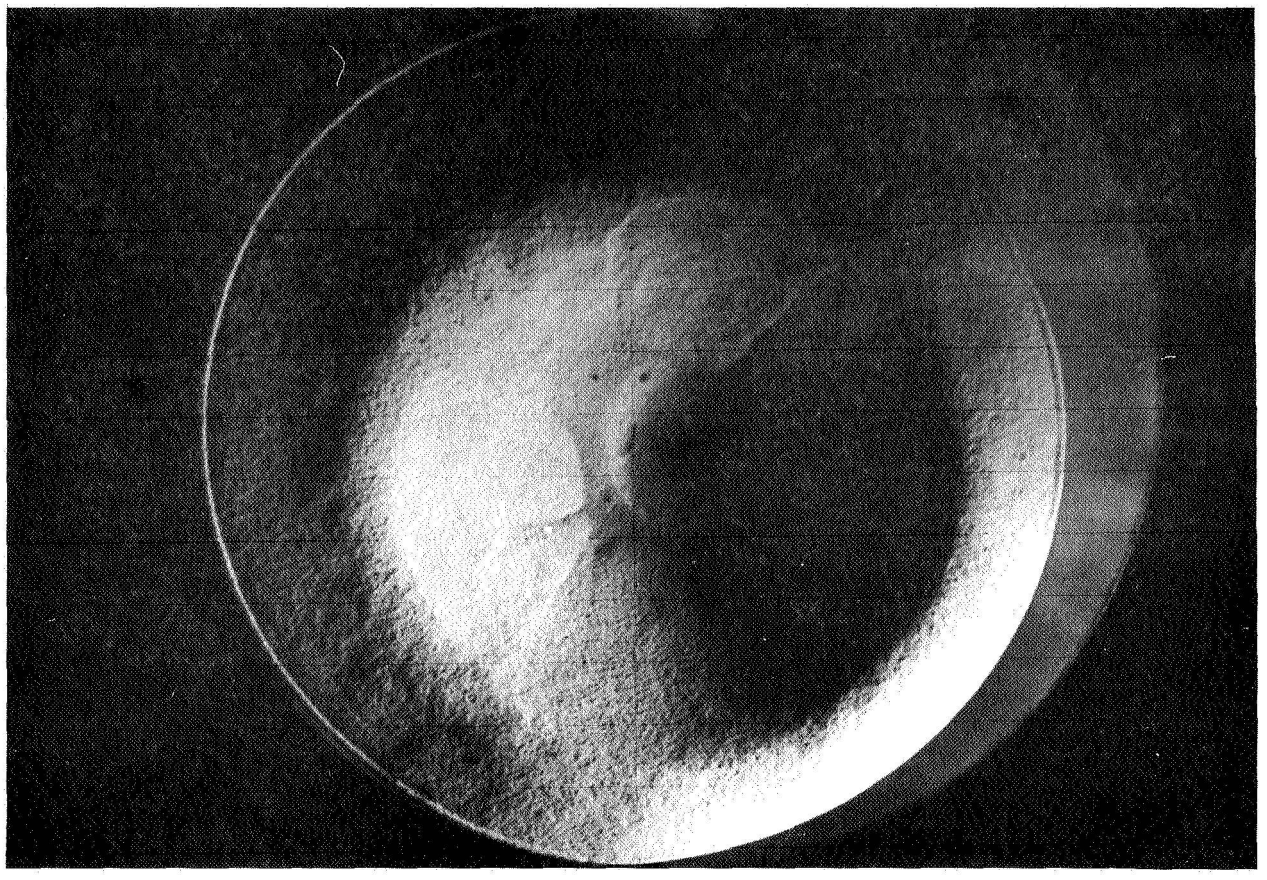

Crater in granular pumice, 62-125 micron size. Medium energy impact. Note fold lines in crater.

Fig. 34

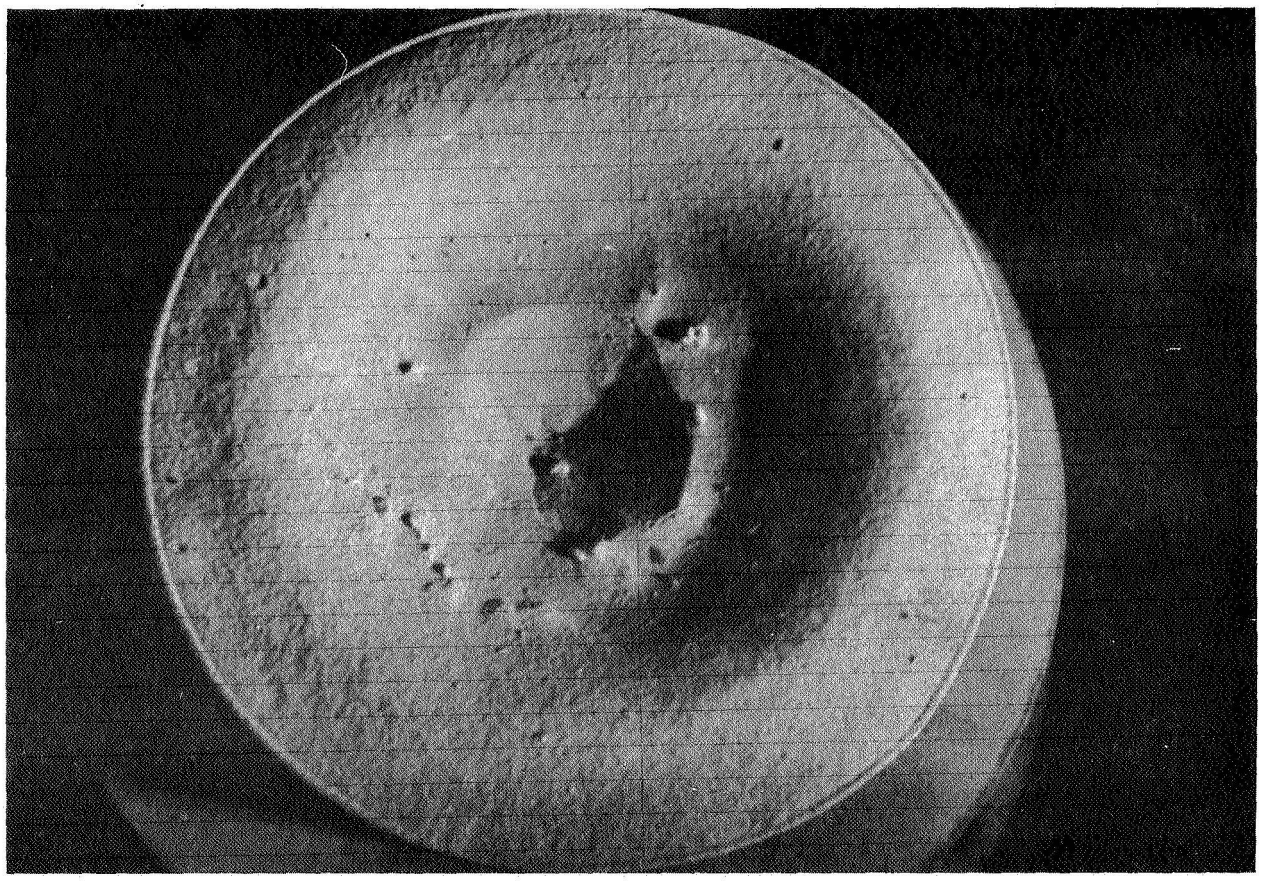

Crater in granular pumice, 62-125 micron size. High energy impact.

Fig. 35

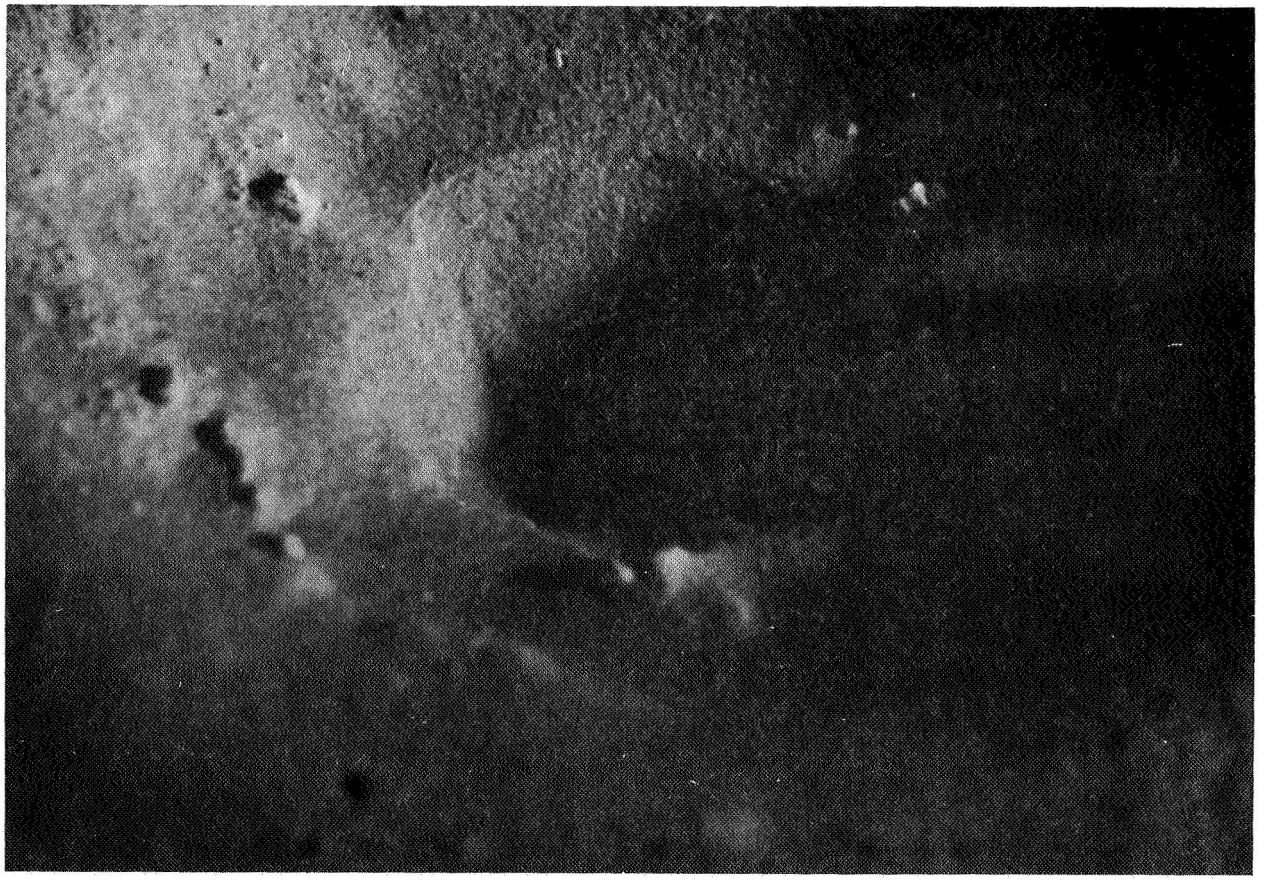

Close-up of central crater in granular pumice, 62-125 micron size. High energy impact.

Fig. 36

Extreme close-up of rim section of central crater in granular pumice, 62-125 micron size. High energy impact.

Fig. 37

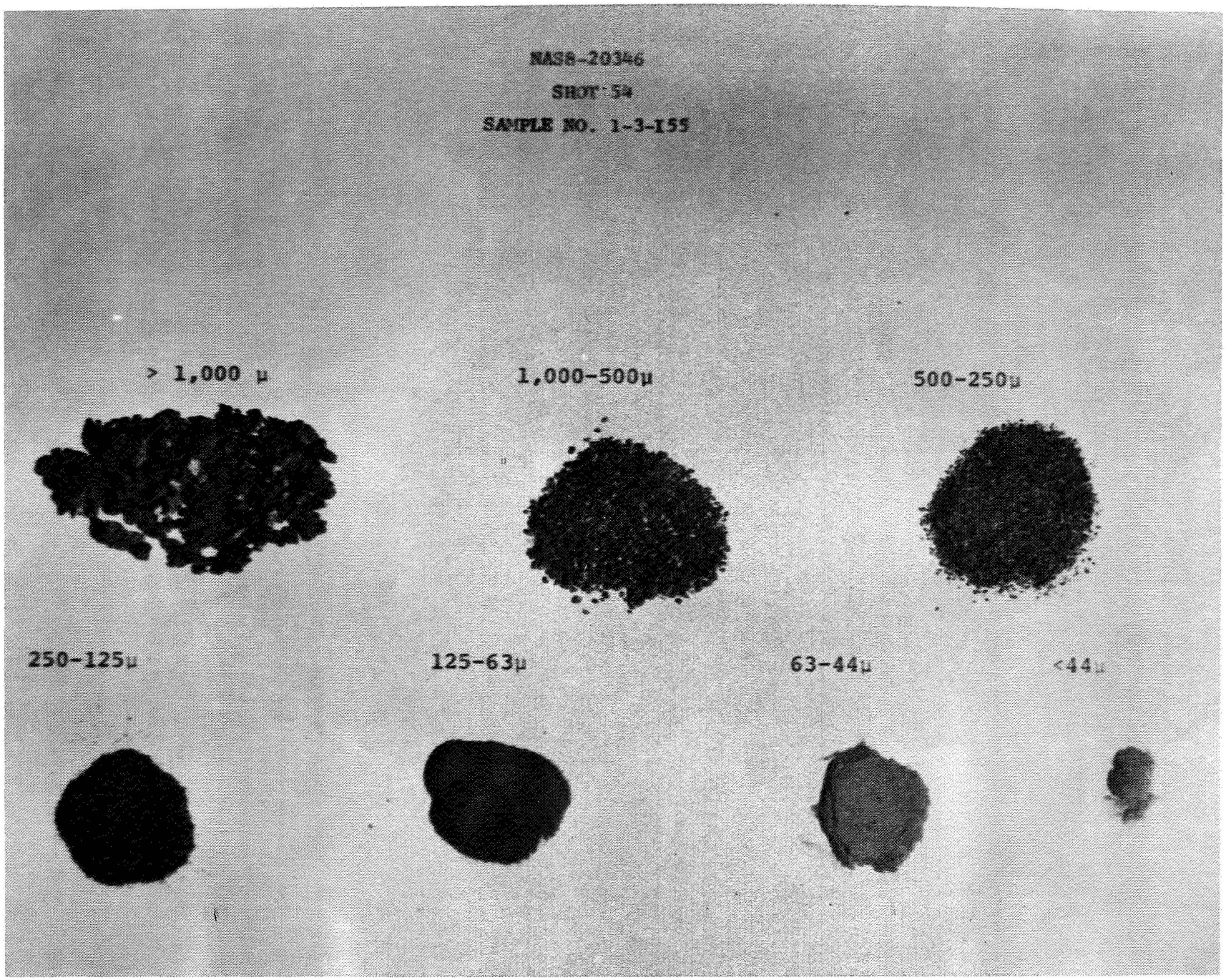
NAS8-20346
SHOT 34
SAMPLE NO. 1-3-155
> 1,000 µ
1,000-500µ
500-250µ
250-125µ
125-63µ
63-44µ
<44µ

Fig. 38

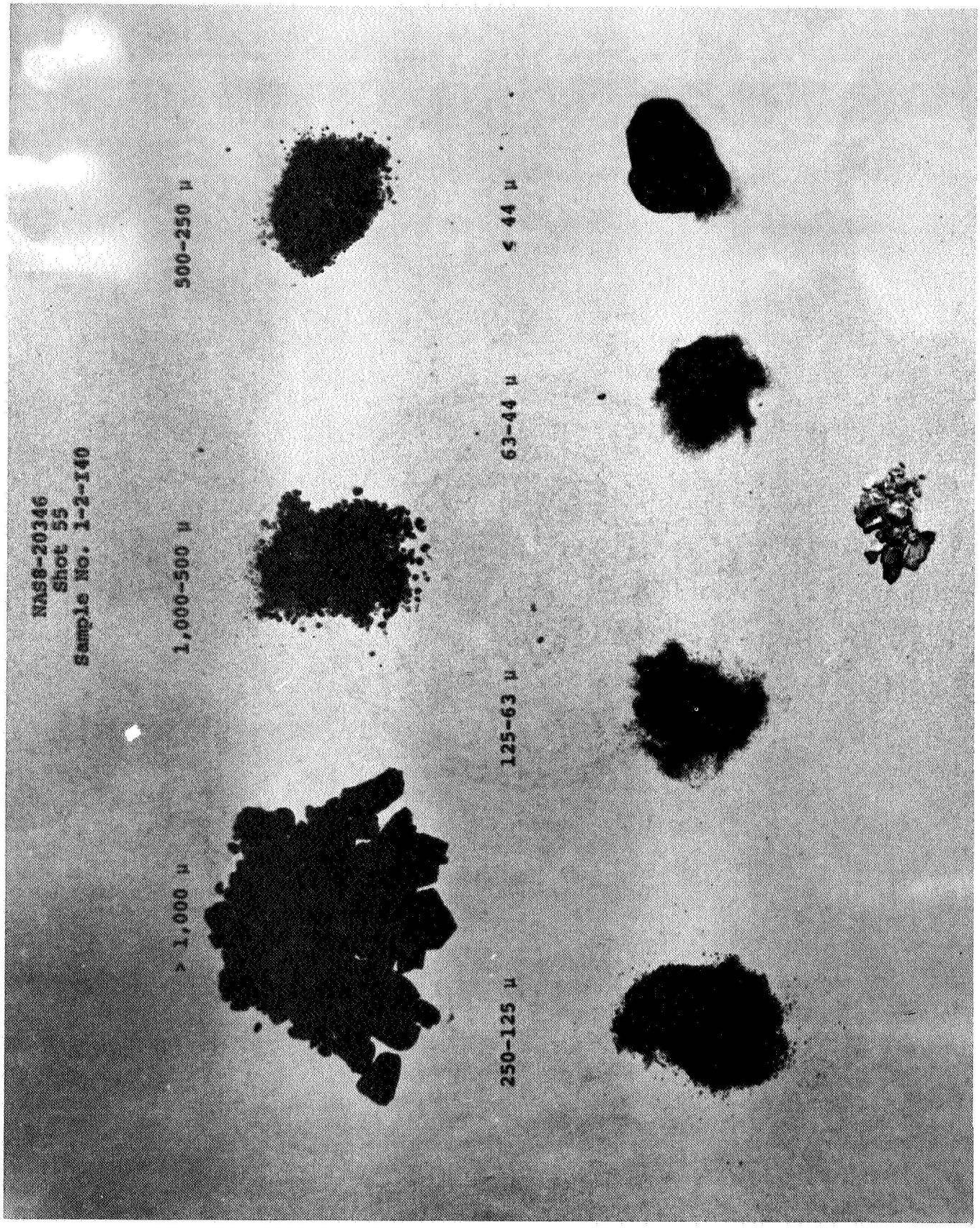
NAS8-20346
Shot 55
Sample No. 1-2-140
< 1,000 μ
1,000-500 μ
500-250 μ
250-125 μ
125-63 μ
63-44 μ
< 44 μ

Fig. 39